Hylan Benton Lyon, Jr.

LOW ENERGY ELECTRON DIFFRACTION STUDY OF LOW INDEX PLATINUM SINGLE CRYSTAL SURFACES

UCRL-17549

UNIVERSITY OF CALIFORNIA

Lawrence Radiation Laboratory
Berkeley, California

AEC Contract No. W-7405-eng-48

LOW ENERGY ELECTRON DIFFRACTION STUDY OF LOW INDEX PLATINUM SINGLE CRYSTAL SURFACES

Hylan Benton Lyon, Jr.

(Ph.D. Thesis)

June 1967

LOW ENERGY ELECTRON DIFFRACTION STUDY OF LOW INDEX PLATINUM SINGLE CRYSTAL SURFACES

Hylan Benton Lyon Jr.

Inorganic Materials Research Division, Lawrence Radiation Laboratory,
and Department of Chemistry,
University of California, Berkeley, California

June 1967

ABSTRACT

The post-acceleration technique of Low Energy Electron Diffraction has been used to examine the three low index (100), (110), (111) crystal faces of platinum. The single crystal samples were subjected to ion bombardment, ultra-high vacuum anneal ($p = 5X10^{-10}$ torr, $25°C < T < 1450°C$) and exposure to different gases (O_2, CO, H_2, CH_4, C_2H_4, NH_3, N_2). The changes in the diffraction features of platinum were correlated to these treatments in an attempt to explain the appearance of new surface structures.

Several distinct sets of new diffraction patterns were observed as a function of these different treatments. These were characterized by the appearance of new periodicities in the diffraction pattern at well-defined ranges of electron beam energy.

A high temperature anneal ($T > 1000°K$) in ultra high vacuum will generally lead to the formation of a disordered, highly unreactive structure which is the same for all three faces of platinum.

The specular intensity was measured as a function of beam voltage.

The Debye temperatures which characterize the mean displacement of the surface atoms perpendicular to the surface planes were measured for all three faces. The average value of the surface Debye temperature is

110°K and shows little variation from face to face. The Debye temperature of bulk platinum is 234°K.

TABLE OF CONTENTS

ABSTRACT iii

I. INTRODUCTION 1

II. EXPERIMENTAL 3

A. The Experimental Technique of Low Energy Electron Diffraction 3

B. The Platinum Single Crystal Sample 32

C. Selected Physical-Chemical Properties of Platinum and Platinum Oxide 35

III. STRUCTURES ON THE (100), (111) AND (110) FACES OF PLATINUM 41

A. General Considerations 41

B. Nomenclature 42

C. Definition of a Clean Surface 44

D. The Effect of Domains 45

E. Surface Structures 46

F. Conclusions 69

IV. ANALYSIS OF EXPERIMENTAL INTENSITY DATA 71

A. General Considerations 71

B. Beam Voltage Dependence of the Specular Intensity 72

C. Comparison of Experiment with Pseudo-Kinematical Theory 82

V. TEMPERATURE DEPENDENCE OF THE SPECULAR INTENSITY (DEBYE-WALLER EFFECT) 87

A. Experimental Results 87

B. Analysis of Results 90

C. Discussion 94

VI. CONCLUSIONS 95

ACKNOWLEDGMENTS 96

APPENDIX A - The Calculation of the Beam Voltage
Dependence of Specular Intensity 97

APPENDIX B - The Calculation of the Debye-Waller Effect 103

REFERENCES 109

I. INTRODUCTION

LEED has provided one of the experimental verifications of the DeBroglie hypothesis. The work of Davisson, Germer,[1] and Farnsworth[2] through the years has provided the foundation for its present application as a major experimental tool in the investigation of the properties of a solid surface. LEED allows us to study the structure of surfaces on an atomic scale. In most of these studies high purity single crystals are used which are studied under ultra high vacuum conditions. The study of single crystal surfaces due to the revivial of this technique is expanding rapidly. During the time in which this work was carried out, the number of LEED research projects has more than quadrupled.

The energy range of the LEED experiment (1-500 eV) provides both the proper wavelength (12 to .5Å) and the limited penetration (1 to 3 atomic layers) which allows these diffraction studies of the surface.

The low index surfaces (100)(110)(111) of single crystal platinum samples have been studied using the LEED technique. Platinum was chosen for this study because it is an excellent catalyst in many surface reactions. A series of experiments using platinum was carried out by Tucker. His work demonstrated the existence of weakly bound, ordered structures, which appeared, on the same low index faces as used in this work, after the exposure to gases. The ambient conditions which were employed in this work were different from those in Tucker's[3] experiment and therefore several diffraction patterns were observed in this work which would not have been observed in the earlier work. We have extended the temperature range of study which permitted us to observe patterns of an entirely different nature.

Experimental results contained herein show the dependence of the structure of the exposed platinum crystal faces to vacuum annealing and to low pressure gas exposure at various temperatures. The evidence for these structures comes from the appearance of extra spots in the diffraction pattern photographs or from the changes of the intensity of the diffraction spots at different beam voltages. There have been several different patterns observed in this work as a function of changing experimental conditions. The experimental conditions and sample preparation are contained in Section II. The study of extra diffraction spots in the LEED patterns as a function of these experimental conditions is contained in Section III.

The understanding of the interaction of a low energy electron beam with the crystal surface is necessary before unique determinations of surface structures can be obtained. To date there has been no general solution for the calculation of intensity of the diffraction features.

The specular intensity maxima as a function of electron voltage have been recorded for the different faces and at different sample temperatures. The results of specular intensity determinations are contained in Section IV.

The attenuation of the intensity of a diffraction maxima as a function of sample temperature (the Debye-Waller effect) has been analyzed. The results of these experiments are contained in Section V.

II. EXPERIMENTAL

A. The Experimental Technique of Low Energy Electron Diffraction

1. The Development of Low Energy Electron Diffraction (LEED)

The first diffraction experiment using low energy electrons (100 eV) was carried out by Davisson and Germer in 1927. The electrons which were back-reflected from the surface of a nickel (nickel oxide) single crystal were collected in a Faraday cup at different angles of scattering. The scattering intensity showed several maxima and minima at well defined angles as predicted by the Laue conditions[4] of diffraction. Thus, this experiment has proved the wave nature of the electron. Using the de Broglie relationship, the electron wavelength, $\lambda(\text{Å})$ is given by $\lambda(\text{Å}) = \sqrt{\frac{150}{V}}$ where V is the accelerating potential in electron volts. The energy range of "low energy" electrons is roughtly 1-500 eV which corresponds to a wavelength range of 12-0.5Å.

The early work of Davisson and Germer was complimented and the experimental technique further developed through the years by Farnsworth. The development of ultra-high vacuum technology,[5] the rediscovery of the post-acceleration detection technique,[6] and the availability of high purity single crystals in recent years have greatly helped to overcome the experimental difficulties. Finally, the availability of a commercial apparatus[7] has further facilitated low energy electron diffraction investigations. These are but some of the reasons for the exponential growth in the number of researchers in the field.

The detailed development of the apparatus is covered in a recent review article.[8] The system used in this investigation was an unmodified Varian LEED apparatus which utilizes the post-acceleration technique.

The diffracted low energy electrons are post accelerated in an electric field (3-7 keV) to impinge on a fluorescent screen. This allows instantaneous view of the entire diffraction pattern which can be monitored continuously during the experiment.

2. The Diffraction Chamber

The requirements of an easily accessible, bakeable, ultra-high vacuum system are best met at present by the all metal copper gasket type system. The schematic in Fig. II-1 shows the relative placement of the equipment for the experiments in this work. The view port allows the entire phosphor screen to be visible. An ion bombardment gun and a quadrupole mass spectrometer were located on opposite sides of the chamber with their centerline axis through the sample. A crystal manipulator was used to position the sample along the centerline axis of the electron optics which is mounted inside the chamber. A 140 L/S ion pump is connected to the chamber through a variable throttle valve. A gas handling manifold, rough pumping system, and a bakeable leak valve, although not shown in Fig. II-1, are also parts of the system. In order to obtain ultra-high vacuum in the diffraction chamber the whole system may be baked at 250°C. In this way the pressure in the system was usually maintained in the low 10^{-10} torr range.

The scheme of the electron optics and the interior of the chamber are shown in Fig. II-2. The electron optics supply a focused beam of monoenergetic electrons which impinge onto the target. The diffraction pattern which appears on the phosphor screen is viewed through the glass, flange mounted, viewport.

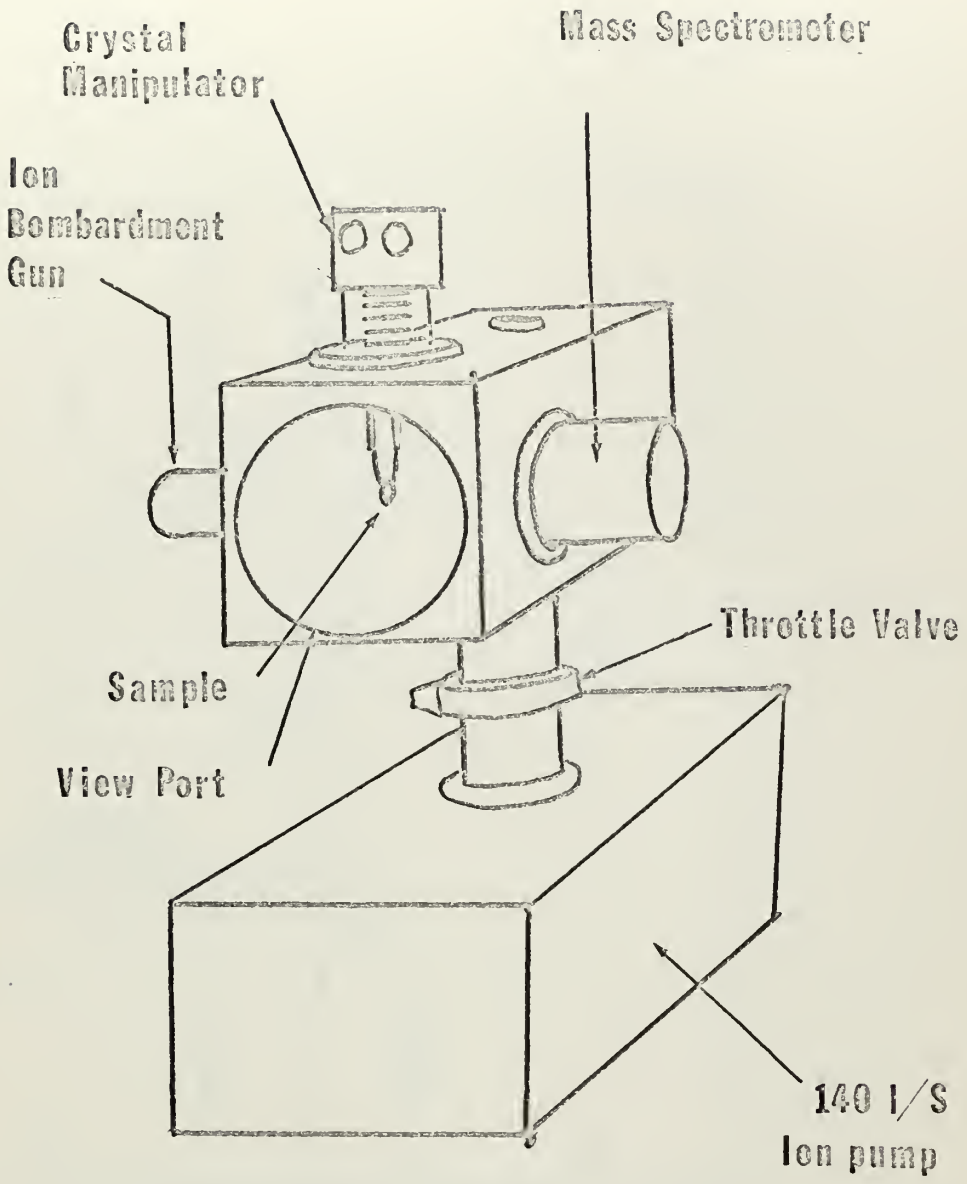

Fig. II-1. Schematic of LEED apparatus showing the location of major components

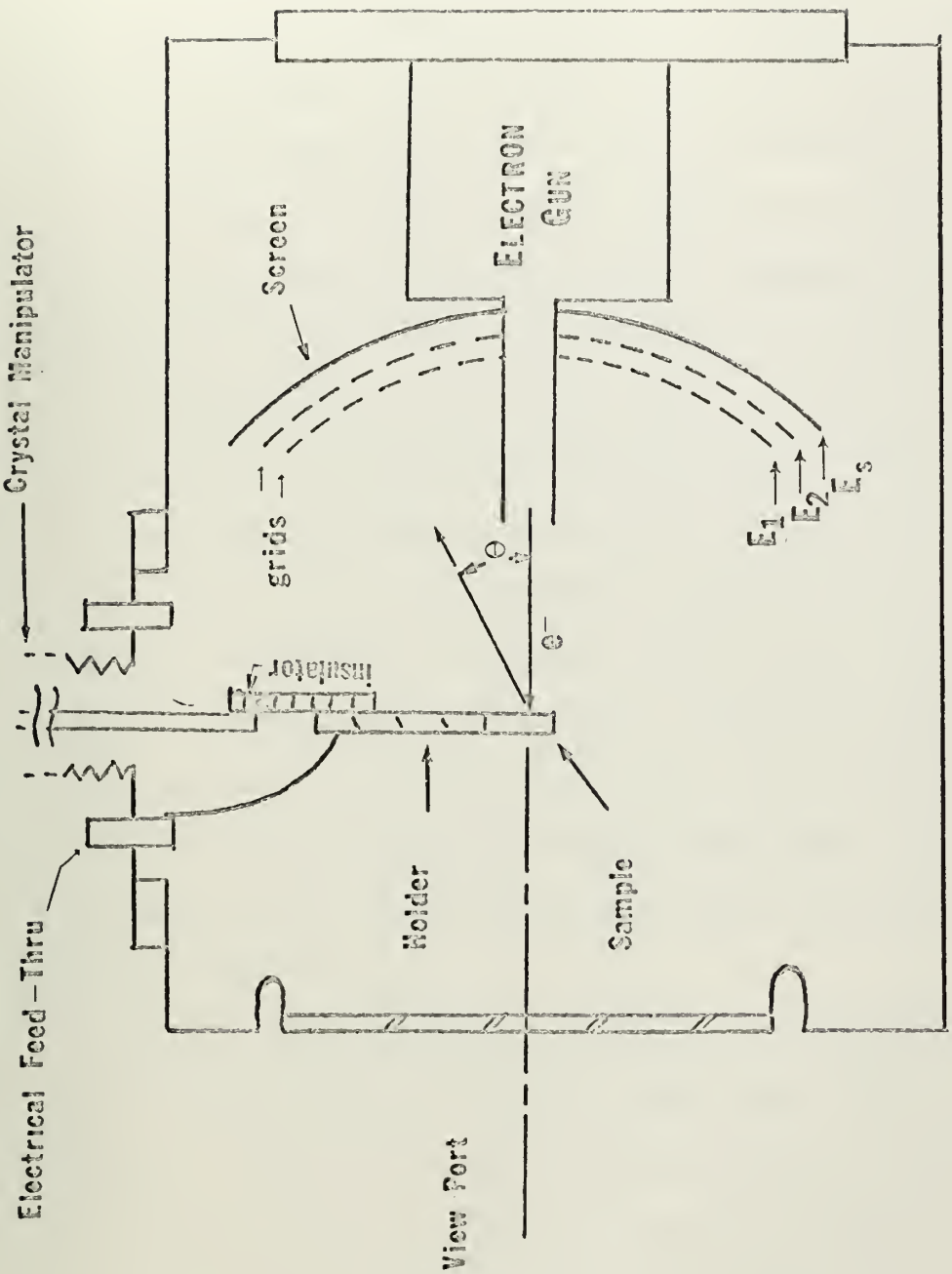

Fig. II-2. LEED chamber detail showing sample placement and electron optics

3. Ambient Conditions

In these studies it is important to control the composition of the background in an ultra-high vacuum system (UHV). In order to determine the composition of the ambient gases in the diffraction chamber, we utilized a quadrupole mass spectrometer mounted as shown in Fig. II-1. The gas atoms entering the ionizer region are ionized by an electron beam of energy (0-90 eV) and the ions are accelerated in a quadrupole field toward a copper-beryllium electron multiplier detector. For a given field condition, only one ion (one m/e ratio) is able to traverse the field without being deflected to the poles. Variation of the quadrupole field allows detection of ions in the 1-500 mass range. This range is divided into three possible ranges, 1-50 amu, 10-150 amu, or 50-500 amu. The sensitivity of this type of equipment is dependent upon the desired resolution. Resolution is a measure of the ability of a mass spectrometer to separate arbitrary mass differences. The greater the resolution desired, the lower the current output for a given partial pressure. The sensitivity observed in this work was a nominal value of 10 amp/torr. For a picoampere of current we could give a rough estimate to a partial pressure of 10^{-13} torr.

A typical mass spectrometer trace which was obtained after baking of the diffraction chamber is given in Fig. II-3. Table II-I gives a summary of the most predominant peaks and assigns a possible species to the peak. In the present work we have based our conclusions upon only uncorrected relative abundances which were directly proportional to the current output from the spectrometer at a given mass number.

One useful determination is to monitor the total pressure with an ion gauge while monitoring the partial pressure of one component with the

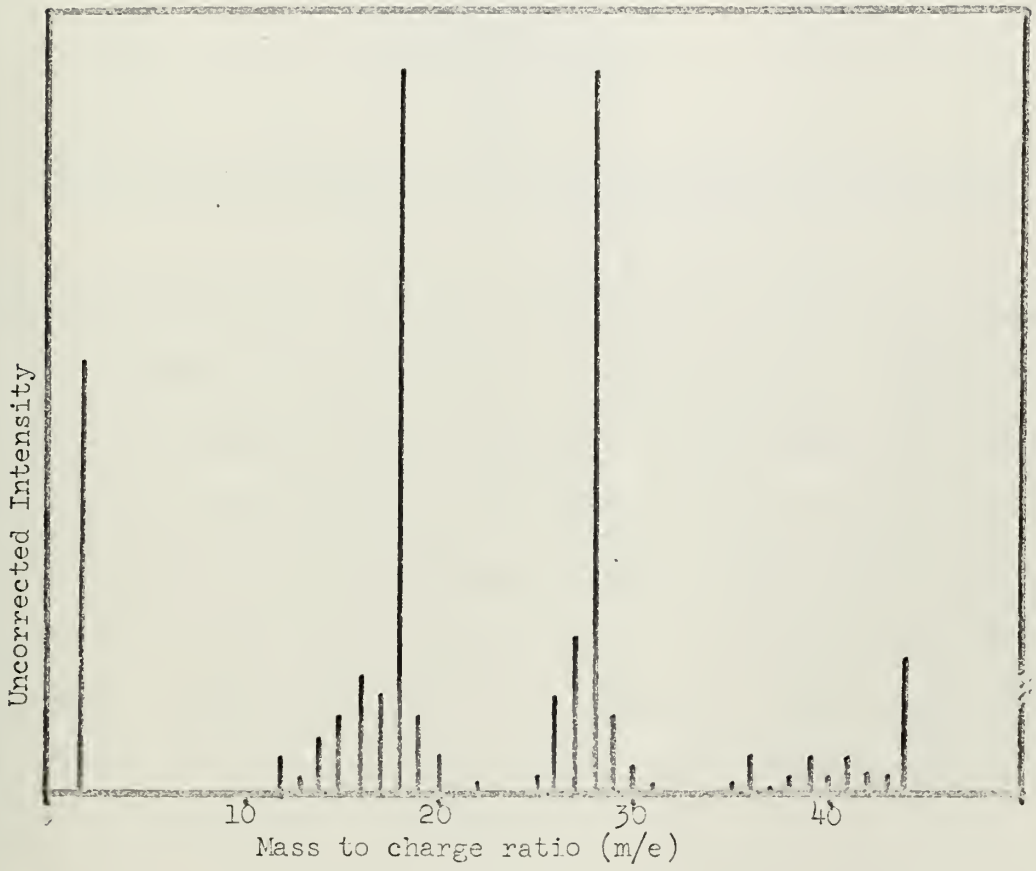

Fig. II-3. Quadrupole mass spectrum (1-45 AMU) of LEED ambient background at $1X10^{-10}$ torr

Table II-I. Mass spectrometric determination of composition

m/e	Species	Uncorrected relative abundance
2	H_2^+	11
16	CH_4^+ O^+	6
17	OH^+	5
18	OH_2^+	18
28	CO^+, N_2^+, $C_2H_4^+$	18
44	CO_2^+	7

mass spectrometer as this gas is admitted to the diffraction chamber. The relationship of total pressure to partial pressure of the gas then measures the effect of system background on the purity of the gas. At high pressures (10^{-8} torr $< p <$ 10^{-6} torr) of the gas, a linear relationship is observed, and at lower pressures the effect of the background becomes predominant. The results of such a determination for methane and for oxygen are shown in Fig. II-4. At pressures greater than $1X10^{-8}$ torr the residual gases comprise a negligible fraction of pure oxygen or methane which was admitted into the diffraction chamber.

The ambient pressure is also dependent on the amount of throttling of the pump. To demonstrate this effect a constant chamber pressure of CO was maintained by varying the gas flow rate to correct for changes in throttle valve settings. CO was chosen because it was the gas which maintained the highest purity when admitted to the chamber.

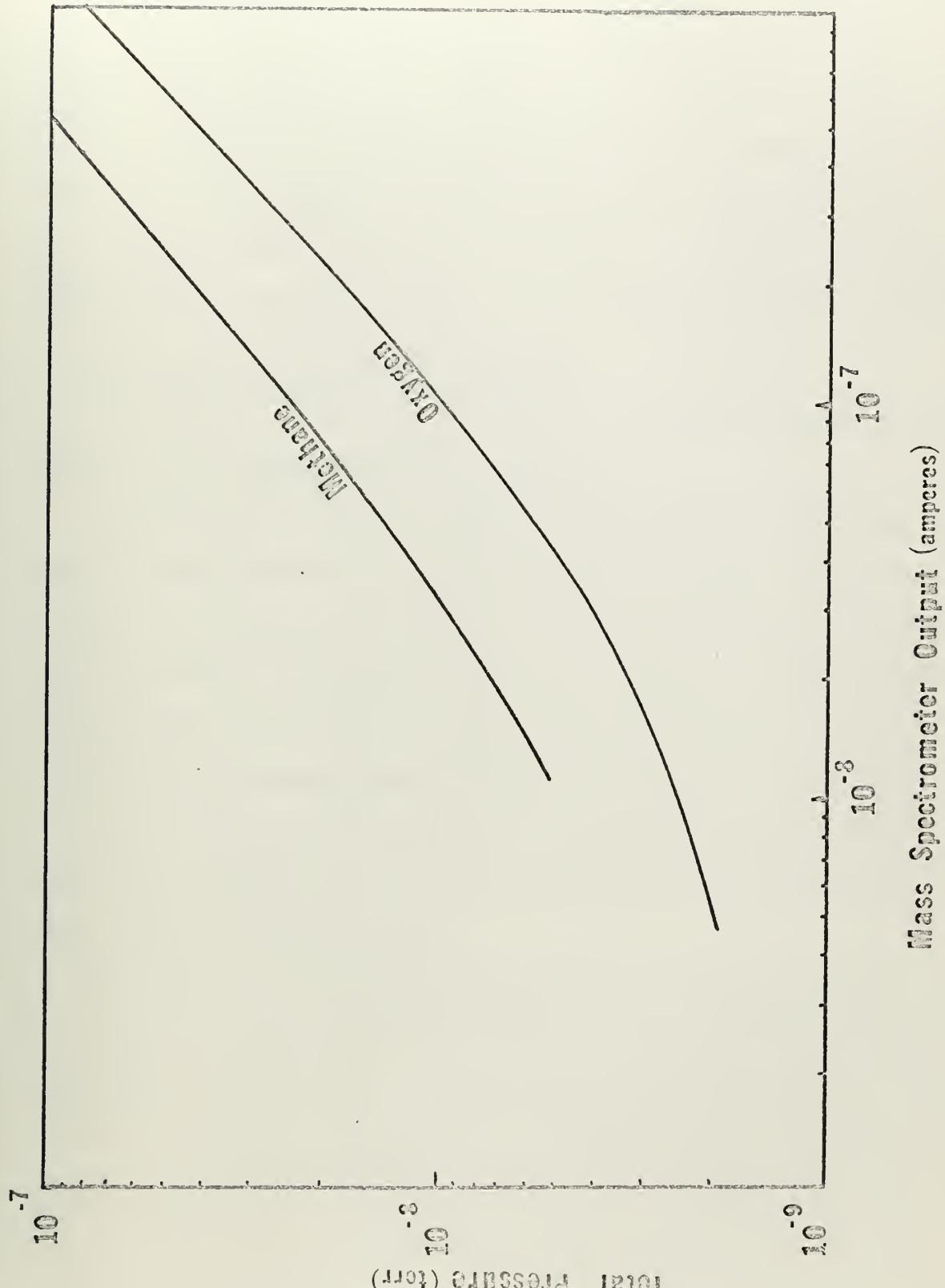

Fig. II-4 Mass spectrometer output for specific m/e as a function of gas backfill pressure

The pressure in the diffraction chamber was maintained at $5X10^{-7}$ torr over a starting pressure of $1X10^{-9}$ torr. At full throttle an uncorrected mass spectrum showed CO to be more than 99.5% of the signal. At no throttle (fully opened valve) the CO pressure was 90% of the total pressure. Therefore, we chose to run gas adsorption experiments using flow rates which correspond to diffraction chamber pressures between $5X10^{-8}$ torr and $5X10^{-6}$ torr with the pump fully throttled. This way we can best preserve the gas purity in our present system during the experiment.

4. Characteristics of the Electron Optics

The electron optics consist of the electron gun, the chamber, the grids, and the phosphor screen (P4 phosphor).

The electron gun (indirectly heatedbariated nickel cathode, electrostatic focusing) produces a collimated beam of electrons of a given voltage. At the sample this beam has a cross sectional area of about 1 square millimeter. The spread of voltage in the beam is stated in the specifications at ±.2 eV at 150 volts. This energy spread was not critical in this work and was not checked during the course of the experiments.

After the electron beam leaves the collimator tube, it is in a field free region as it travels to the sample and back to the first grid (labelled F_1 in Fig. II-2).

The electrons then pass through the first grid and are retarded by a repulsive potential (F_2 in Fig. II-2) which is equal to the original accelerating potential (eV). The electrons which have sufficient energy to pass this repulsive potential are then accelerated by an attractive potential (F_S in Fig. II-2) of usual value 5 kV. In this manner the electrons which scatter off the sample without losing energy (elastic electrons) are separated from the inelastically scattered electrons and

are displayed on the phosphor screen at intensities visible to the naked eye. The energy of the beam is variable in a range from 0-500 eV. The current density impinging on the crystal is in the range of 1-10 μamps, and it depends on the accelerating potential.

The beam of electrons incident upon the crystal is monoenergetic for our purposes. Let a vector J_o describe the magnitude of flux of electrons as well as their direction. The reflected electronic current can be designated J_r and is not monoenergetic. If there is a net difference in these two currents then there must be a current in the crystal to ground circuit.

The crystal to ground circuit current, designated ΔJ, is a function of the energy of the incident electrons. A value for this current can be plotted out as a function of beam voltage and is shown in Fig. II-5 as the solid line. The electron beam voltage at which the current ΔJ equals zero is called the cross-over voltage. This is where the crystal to ground current is zero and is related to the secondary electron emission ratio. This cross-over voltage (E_c) varies slightly and has been observed to change by as much as 10-20 eV. An attempt to correlate this to gas coverage was unsuccessful.

Secondary electron emission was the subject of great interest in the 1920-1930 period. From this era this ratio for platinum has been recorded[9] and the dashed curve in Fig. II-5 shows the comparison. The data plotted were derived from the values of σ, the secondary electron emission coefficient as follows:

$$\Delta J = J_o - J_r = J_o - \sigma J_o = (1-\sigma)J_o$$

We were unable to determine the absolute value of J_o but we could determine experimentally its relative value from its voltage dependence.

$$J_o \propto 2(eV) + 0.170\ (eV)^2$$

The plotted curve is therefore,

$$\Delta J_{(eV)} \propto (1-\sigma)(2eV + 0.170\ eV^2)$$

We could show experimentally that $\Delta J_{(eV)}/J_o$ was independent of the magnitude of J_o. We can then assume we have a very sensitive measure of the cross-over voltage.. Without establishing the absolute value of J_o we cannot determine secondary electron emission values at other than this cross-over voltage. This effect is important in two cases, one where the target is an insulator and also where the sample is not grounded. In either of these cases the sample will "charge up" and the electrons will not hit the crystal unless the beam voltage is above the cross-over voltage.

The experimental apparatus allows a measurement of the energy distribution of the reflected beam J_r. This distribution is obtained by varying the voltage of the repeller grid (E_2 Fig. (II-2)) and collecting the screen current while holding the beam voltage constant. The screen current is then recorded as a function of E_2. Differentiating this curve yields a relative measure of the amount of electrons within a given spread of E_2. This assumes that the energy distribution collected by the screen ($\theta = \pm 47.5°$) is the same as energy distribution which would be measured

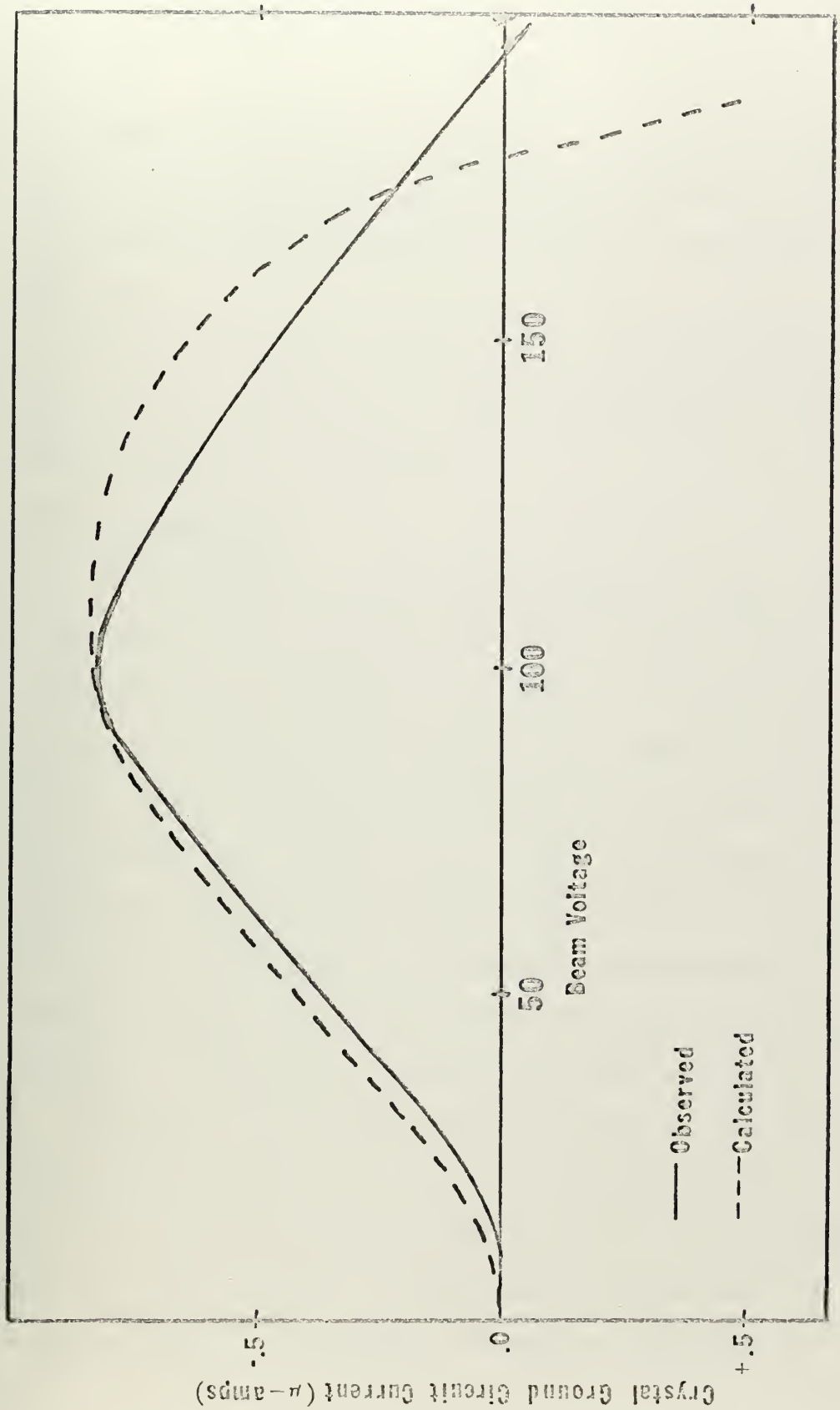

Fig. II-5 Crystal to ground circuit current as a function of beam voltage

if all the back scattered electrons were collected ($\theta = \pm 90°$). The results of such a determination at 100 eV beam voltage are given in Fig. II-6.

From these experiments we can also determine the percentage of elastic electrons at this voltage. The measurements are then carried out at many different voltages. The results of this study are shown in Fig. II-7.

We have also measured this ratio of elastic to inelastic electrons as a function of temperature. Within the accuracy of our experiment this ratio is temperature independent.

5. Ion Bombardment

Ion bombardment is used in this experiment to remove damaged surfaces or unwanted surface species by sputtering. This technique is used to remove the surface damage which is introduced during the preparation of the single crystal samples. The inability to form a single crystal surface prior to placing the sample in the chamber does not prevent investigators from carrying out the experiment. A series of bombardments and high temperature anneals can remove the damaged atomic layers at the surface and expose an ordered surface. The experiment can begin on this freshly prepared surface. Thus, one of the main advantages of the ion bombardment technique is the ability to prepare the crystal surface in situ.

Bombardment is usually carried out by filling the chamber to a xenon pressure of $1X10^{-5}$ torr. Xenon was used because it has a greater mass than that of argon and thus a greater momentum exchange which increases its sputtering efficiency. It can also be removed easier by the vacuum ion pump than argon.[10] The chamber ion pump was turned off and within one hour

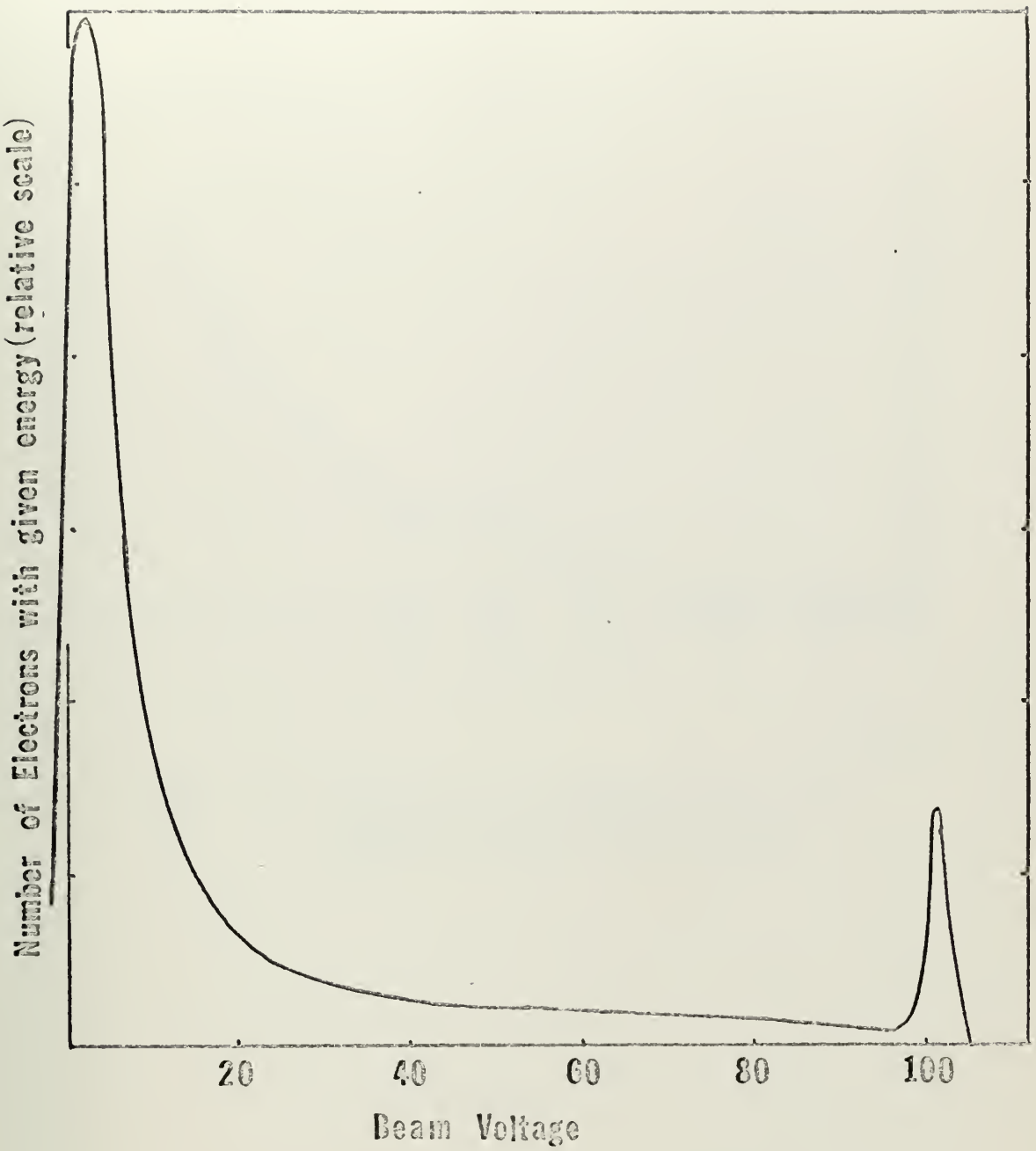

Fig. II-6. Energy distribution of reflected electrons on Pt(100) face for 100 volt incident energy

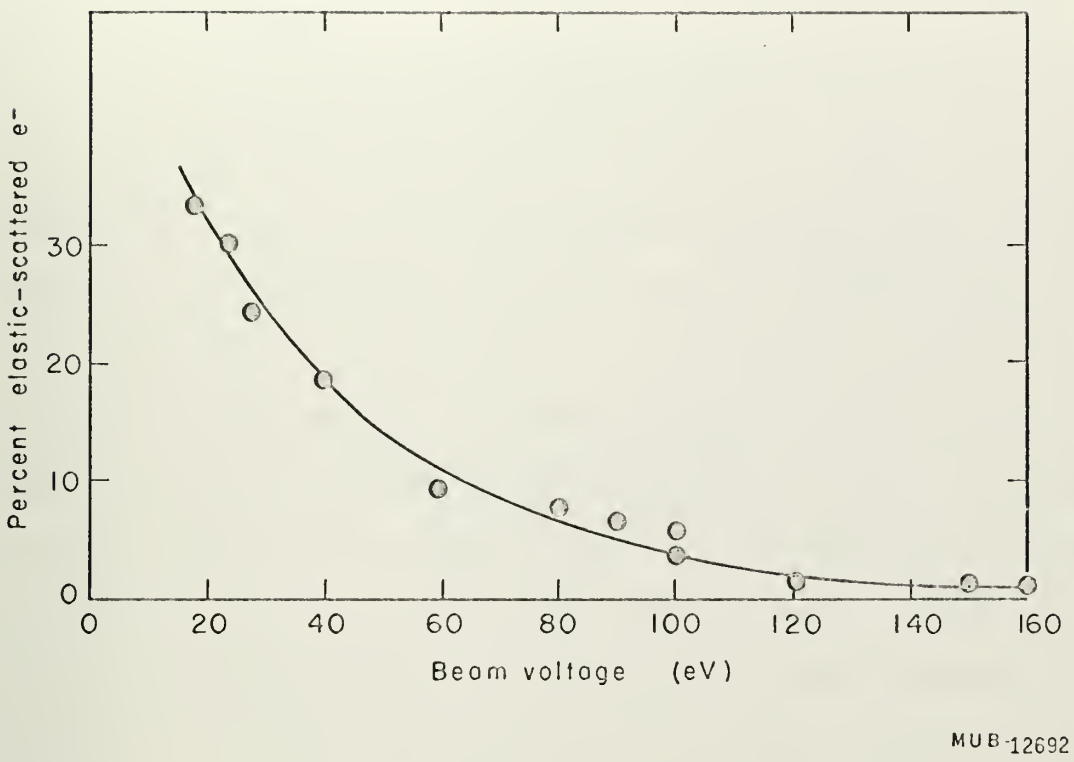

Fig. II-7. Percentage of reflected current which undergoes elastic reflection as a function of incident beam energy

pressure nominally stabilized at $1X10^{-6}$. The spectrum was checked by mass spectrometer and found for all practical purposes to be entirely xenon and argon. Then the system pressure was increased by admitting xenon to $1X10^{-5}$ torr.

The ion beam energy can be varied in the range of 140-340 eV. Due to the geometry of the system this ion beam could be analyzed in the mass spectrometer without the use of the mass spectrometer ionizer section. An estimate of the composition of the ion beam may be obtained from the spectra shown in Fig. II-8. The loss of resolution in this spectra is due to the high energy of the particles (140 eV). Note that the largest signal is Xe^+ which was measured to be more than 4 orders of magnitude over the intensity of the species shown. In this particular recording the Xe^+ peak saturated the logarithmic amplifier used to record the signal. From such a determination it is certain that the major component of the beam is Xe^+ ions which are responsible for the gross change of the crystal surface characteristics after ion bombardment.

The properties of this particular apparatus are such that changing the beam voltage does not change the flux of the beam. The ΔJ value mentioned earlier for electrons can be measured during ion bombardment of the crystal by Xe^+. Figure II-9 shows that the crystal ground circuit current changes by a factor 1.5 over the energy range, 140-340 eV. For this specific reason no estimate of the ions/sec incident upon the sample is given since the mechanism of the interaction is unknown. We did not have a method of relating this crystal to ground circuit current to an effective beam current. If such a method had been available, it would have been possible to establish a parameter which would permit the number of Xe^+ ions that were incident upon a given area to be calculated as a function of time.

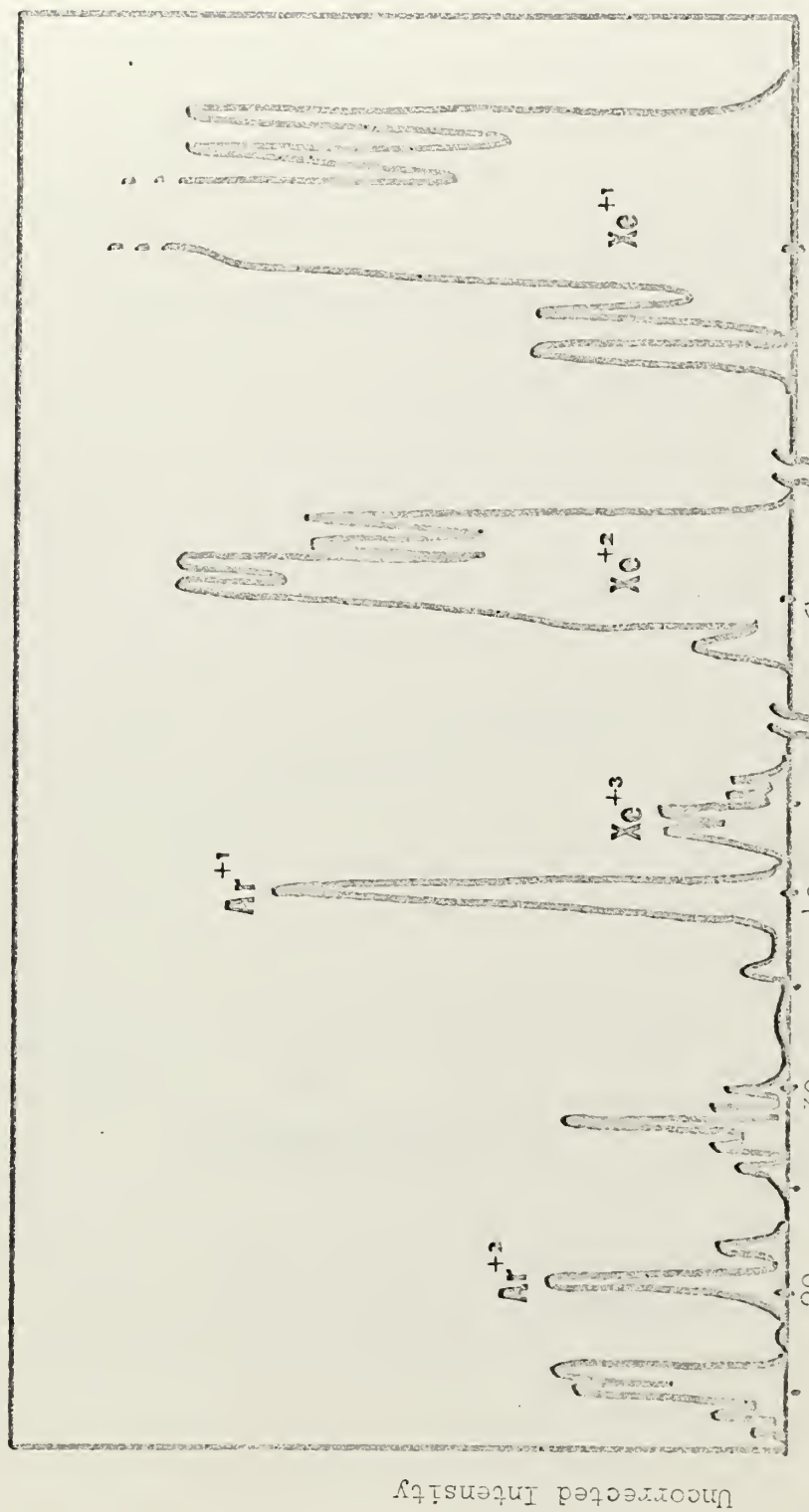

Fig. II-8. Quadrapole mass filter determination of composition of ions in the ion bombardment beam for 140 volt Xe ion bombardment

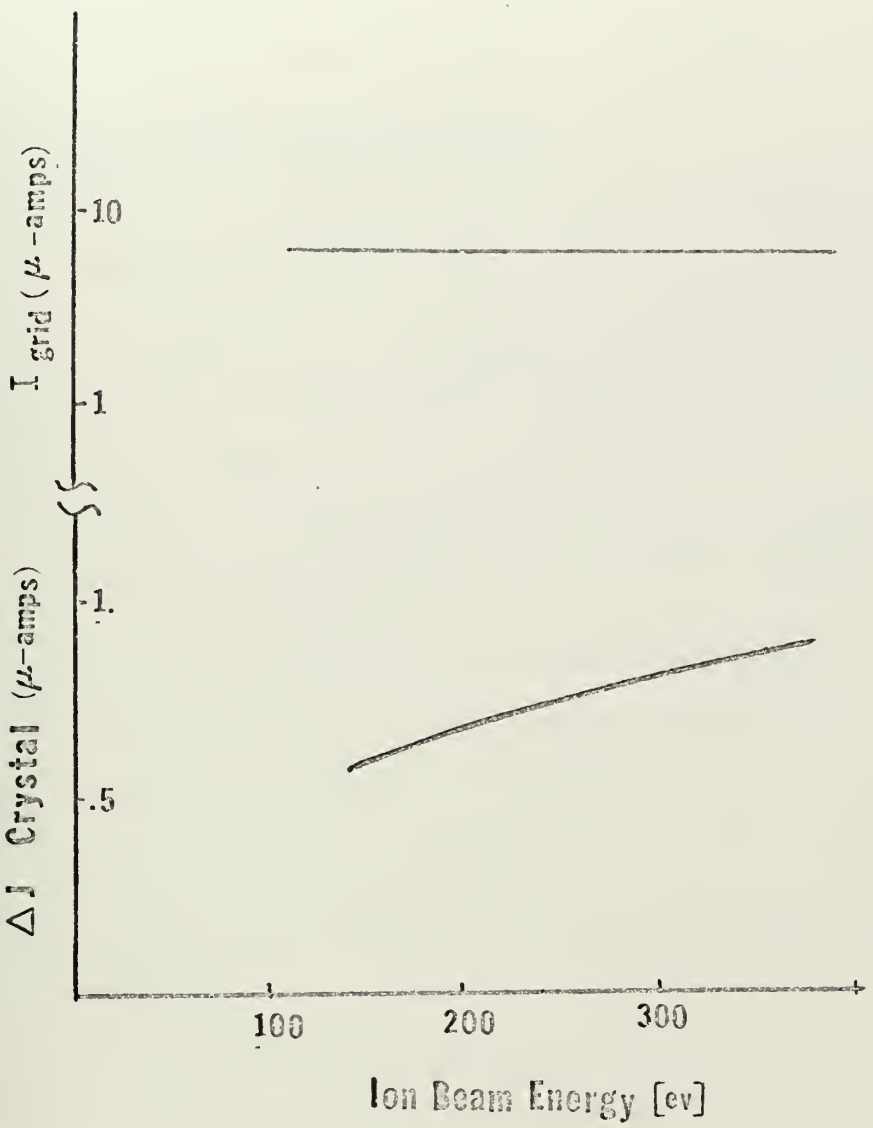

Fig. II-9. Plots of relative beam intensity (I_{grid}) and crystal to ground circuit current (ΔJ) as a function of Xe ion beam energy

Reproducibility was achieved by standardizing the conditions for bombardment. Ion bombardment treatments using 340 eV Xe ions in a back pressure of 1×10^{-5} torr Xe were carried out for 15 minutes in order to remove unwanted diffraction features. The sample was positioned into the beam by maximizing the crystal to ground circuit current.

6. Crystal Manipulator and Sample Holder

The crystal sample was spot welded to the holder material which was mounted with pressure contact onto the crystal manipulator (Fig. II-1). The bellows arrangement on the maniuplator allowed full (360°) rotation of the holder. This was limited however to 180° by the necessary electrical connections to the sample.

The samples were heated by resistance heating of the sample and the holder. In order to obtain high temperature (>1200°C) with reasonable currents (40 amps), the sample holder was made much thinner than the sample cross sectional area. The sample holder became the heat source and a steady state sample temperature was achieved much faster and used much less current than required by other methods.

The holder material was made of platinum which allowed etching of the sample after mounting.

The crystal maniuplator allowed for vertical, sidewards, and tipping motion, within limits, and varying the sample position with respect to the impinging electron beam. It is also important to locate the sample at the center of curvature of the spherical screen if angle determinations are expected. The system as used met the demands placed upon it for the level of accuracy required in this work. Temperatures from room temperature to 1350°C were recorded by a Pt/Pt 10% Rh thermocouple attached to the back of the sample. The samples were easily adjusted to be with the electron beam incident upon the desired portion of the face.

7. Intensity Measurements

The diffraction pattern which is displayed on the phosphor screen can directly be photographed to obtain permanent record of a given diffraction feature. It takes approximately 3-5 sec to form an adequate image on ASA 3000 film. The relative intensities of the diffraction spots can then be determined by techniques which are to be described later in the photographic section. The direct measurement of the intensity of the individual diffraction spots can be accomplished by the use of spot photometers. The majority of intensity data in this work were recorded with a spot photometer. The photometer used has fiber optics allowing the use of variable apertures by varying the size of fibers.

a. Determination of electron flux from intensity measurements. The Faraday cup method of scanning electron diffraction patterns can be used to determine the absolute electron flux.

Intensity measurement using the fluorescent screen can only be used to determine relative intensities. The problem in the post acceleration method is to relate the spot photometer reading to the intensity that a Faraday cup would receive at the same position of measurement. The intensity at any position on the screen will be identified by its θ,ϕ coordinate on a corresponding photograph as $I_{(\theta\phi)}$. Unfortunately $I_{(\theta\phi)}$ is not comprised only of the electrons scattered into the diffraction maxima. The total intensity at any point (θ,ϕ) is given by the following relationship.

$$I_{(\theta\phi)} = I_{diff} + I_{T.D.S.} + I_{disorder} + I_{inelastic} + I_{optical}$$

The various terms are important to consider separately.

I_{diff} - This term gives the intensity due to elastically scattered, diffracted electrons after thermal effects have been taken into account.

$I_{T.D.S.}$ - This term is the intensity due to elastic electrons scattered as a result of thermal motion (Debye-Waller factor) of the lattice.

$I_{optical}$ - represents that fraction of the total intensity reaching the spot photometer from outside the scanned area. Intensity at other positions may be recorded due to insufficient cut-off by the telephotometer optics or optical reflections.

$I_{disorder}$ - If all atoms are in disordered positions, no diffraction pattern will appear. This term then accounts for the intensity of electrons scattered from atoms which are in disordered positions. When the surface approaches perfect crystallinity, $I_{disorder}$ almost completely vanishes. Immediately after ion bombardment treatments of the surface $I_{disorder}$ is very large.

$I_{inelastic}$ - This term is due to the fact that the retarding potential grid (E_2) does not remove all of the inelastically scattered electrons due to the accelerating voltage (5 KV) of the screen. This is an instrumental effect which can be reduced by lowering the screen potential or by the insertion of another grid.

I_{diff} I_{TDS} and $I_{disorder}$ are proportional to the electron flux. The other terms are due to a mixture of instrumental errors. In analyzing spot intensity data the presence of these factors which can have an effect on the calculation of electron flux $J(\theta,\phi)$ and which can also be a function of the experimental conditions cannot be overlooked.

b. Specular intensity as a function of temperature. If the intensity of the specular reflection is recorded as sample temperature is changed, the value of I_{diff} will change, see Fig. II-10. The background intensity remains constant and must be subtracted from the total intensity $I_{(\theta, \phi)}$ to obtain a more accurate measure of I_{diff}.

8. Photographic Measurements

The phosphor screen was directly photographed through the viewport using a Crown Graphic camera which was mounted in a fixed position with respect to the screen as shown in Fig. II-11. This positioning allowed an acceptable depth of field with an f-stop of 8 or 11.

Exposure times for normal patterns were of reasonable duration allowing several types of films to be used. Table II-II gives the approximate conditions which were used with the various films in obtaining photographs of the platinum diffraction pattern.

The faster film made by Polaroid (Type 57) was used to determine the proper exposure for the existing condition. Then the time of exposure was increased by the time calculation factor listed in Table II-II, when other films were employed. Films which produce negatives were used with micro densitracers to obtain intensity data. The diffraction angle θ can be obtained from the location of the diffraction spot image on the negative.

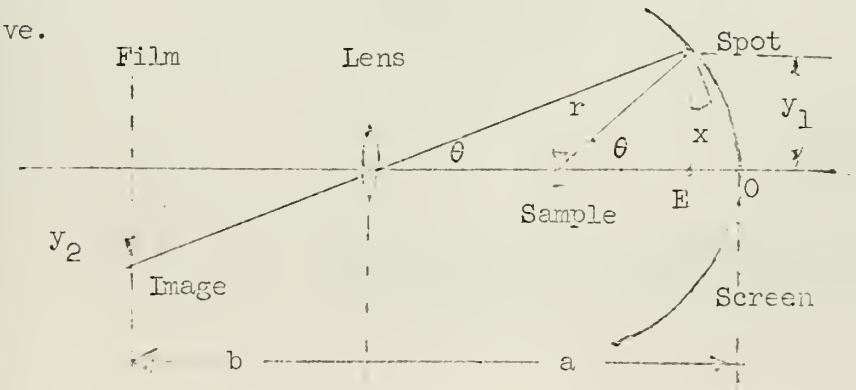

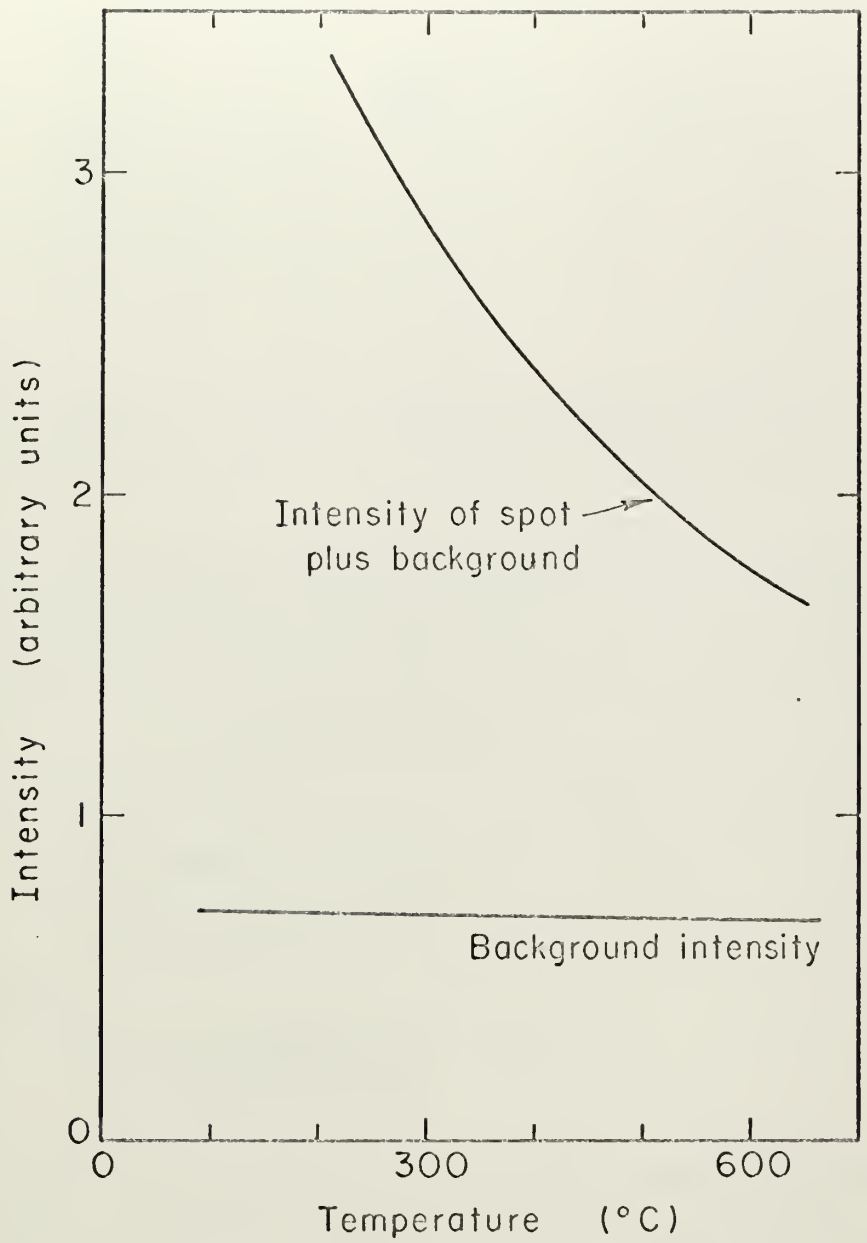

Fig. II-10. Intensity of the specular reflection of a diffraction pattern as a function of temperature

Table II-II

Film Size	Film Type	ASA	Exposure Time	f stop	negative	Time Calc. Factor
4X5	Polaroid 57	3000	1 sec	8	no	1
4X5	Polaroid 55	50	60 sec	8	yes	60
4X5	Royal Pan	400	8 sec	8	yes	7.5
70 mm roll	Tri-X-Pan	1200	4 sec	8	yes	3

Given the preceding geometry the derivation of an equation to calculate y_2 in terms of θ is as follows:

$$y_1 = r \sin\theta = (a-OE) \tan$$

$$y_2 = b \tan$$

$$X = \theta/2$$

$$OE = y_1 \tan \theta/2$$

which leads to

$$y_2 = \frac{br \sin \theta}{a-2r \sin^2 \theta/2}$$

This derivation neglects the effect of the refraction due to the view port. The parameter y_2 is in centimeters if r, b and a are measured in centimeters. The actual distances in centimeters which were used in this work are shown below.

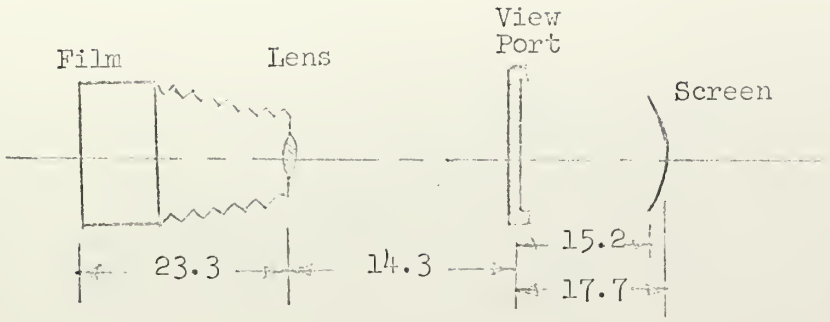

Fig. II-11

This parameter y can be calculated for the given conditions as a function of θ.

It is useful to express θ in terms of a dimensionless parameter, y_r. This parameter (y_r) is defined as (y_2) divided by the radius of the screen (y_{max}) projected onto the film.

$$y_{max} = \frac{br \sin (47.5)}{a\text{-}2r \sin^2 (23.7)}$$

or

$$y_r = \frac{(a\text{-}2r \sin^2 (23.7)\ ) \sin \theta}{\sin (47.5)\ (a\text{-}2r\sin \theta/2)}$$

Using this expression film shrinkage, enlargement or possible change in film to screen distance may not make recalculation of θ and y_2 necessary. Values for y_2 and y_r have been calculated as a function of theta and are listed in Table II-III.

In these calculations we have assumed that the sample is at the center of the radius of curvature of the screen (r = 7 cm). A correction must be applied to allow for the change of θ if the sample is not in the center of curvature, that is, the sample to screen distance is either

larger or smaller than 7 cm. If we consider x to be the displacement from the center of curvature then,

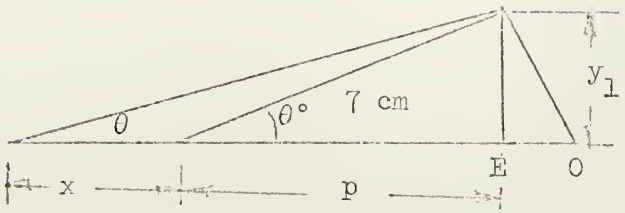

$$y_1 = 7 \sin \theta^\circ \qquad p = 7 \cos \theta^\circ$$

$$\tan \theta = \frac{y_1}{x+p} = \frac{7 \sin \theta}{x+7 \cos \theta^\circ} = \frac{\sin \theta^\circ}{\frac{x}{7} + \cos \theta^\circ}$$

$$\theta = \text{arc tan} \left\{ \sin \theta^\circ / (\tfrac{x}{7} + \cos \theta^\circ) \right\}$$

The error in measuring the angle is then going to be dependent not only on the displacement but on the angle θ. The ratio $x/7$ will be small compared to unity, so at small angles $\theta \approx \theta^\circ$. At larger angles a small error in the placement of the sample gives a large error in the value of θ. For a placement error of 5 mm the error made in measuring the angle θ is plotted in Fig. II-12.

Figure II-14 and Fig. II-13 give the results of calculations which correct for placement errors. It is necessary to point out that in practice it is difficult to measure the placement parameters (y_r) to more than 5% accuracy and as a result angle determinations have large uncertainties ($\pm .5^\circ$).

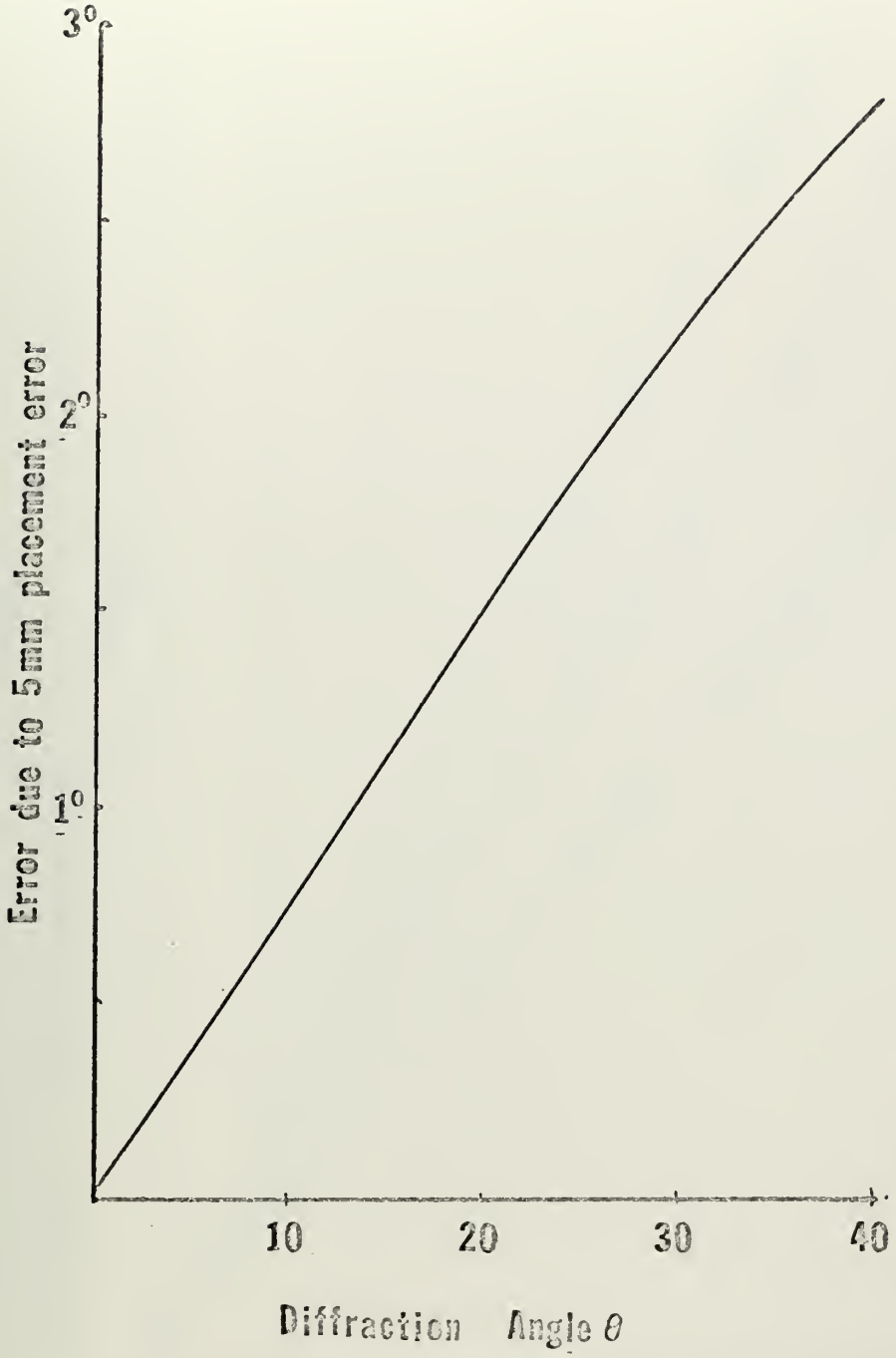

Fig. II-12. Error in measurement of angle due to unaccounted error in spacing of 5 mm

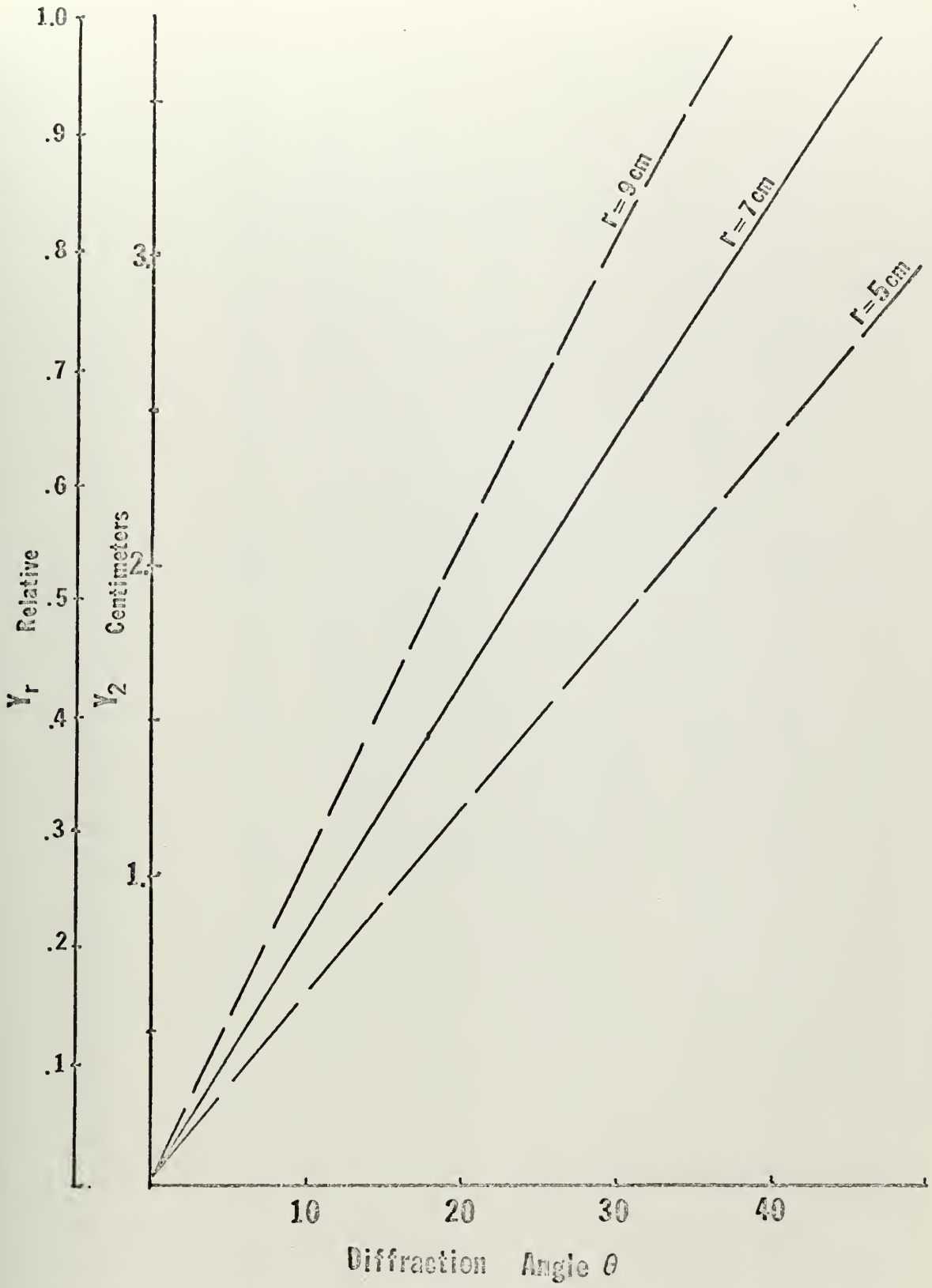

Fig. II-13. Film position of spot as a function of diffraction angle θ

θ for various sample to screen distances

y_2(cm)	y_r	r=9.0	8.5	8.0	7.5	7.0	6.5	6.0	5.5	5.0
.17	.044	1.6	1.6	1.8	1.9	2.0	2.2	2.3	2.5	2.8
.25	.066	2.3	2.5	2.6	2.8	3.0	3.2	3.5	3.8	4.2
.33	.088	3.1	3.3	3.5	3.7	4.0	4.3	4.7	5.1	5.6
.41	.110	3.9	4.1	4.4	4.7	5.0	5.4	5.8	6.4	7.0
.50	.132	4.7	4.9	5.3	5.6	6.0	6.5	7.0	7.6	8.4
.58	.154	5.4	5.8	6.1	6.5	7.0	7.5	8.2	8.9	9.8
.66	.176	6.2	6.6	7.0	7.5	8.0	8.6	9.3	10.2	11.2
.75	.198	7.0	7.4	7.9	8.4	9.0	9.7	10.5	11.4	12.6
.83	.220	7.8	8.2	8.8	9.3	10.0	10.8	11.7	12.7	14.0
.91	.242	8.6	9.1	9.6	10.3	11.0	11.8	12.8	14.0	15.3
.99	.264	9.3	9.9	10.5	11.2	12.0	12.9	14.0	15.2	16.7
1.07	.286	10.1	10.7	11.4	12.1	13.0	14.0	15.1	16.5	18.1
1.16	.307	10.9	11.5	12.3	13.1	14.0	15.1	16.3	17.8	19.5
1.24	.329	11.7	12.4	13.1	14.0	15.0	16.1	17.5	19.0	20.9
1.32	.351	12.5	13.2	14.0	15.0	16.0	17.2	18.6	20.3	22.2
1.40	.373	13.3	14.0	14.9	15.9	17.0	18.3	19.8	21.5	23.6
1.48	.394	14.0	14.9	15.8	16.8	18.0	19.4	20.9	22.9	24.9
1.57	.416	14.8	15.7	16.7	17.8	19.0	20.4	22.1	24.0	26.3
1.65	.437	15.6	16.5	17.5	18.7	20.0	21.5	23.2	25.3	27.6
1.73	.459	16.4	17.3	18.4	19.6	21.0	22.6	24.4	26.5	29.0
1.81	.480	17.2	18.2	19.3	20.6	22.0	23.7	25.5	27.7	30.3
1.89	.502	18.0	19.0	20.2	21.5	23.0	24.7	26.7	29.0	31.6
1.97	.523	18.7	19.8	21.1	22.4	24.0	25.8	27.8	30.2	33.0
2.05	.544	19.5	20.7	22.0	23.4	25.0	26.9	29.0	31.4	34.3
2.13	.566	20.3	21.5	22.8	24.3	26.0	27.9	30.1	32.7	35.6
2.21	.587	21.1	22.3	23.7	25.3	27.0	29.0	31.3	33.9	36.9
2.29	.608	21.9	23.2	24.6	26.2	28.0	30.1	32.4	35.1	38.2
2.37	.629	22.7	24.0	25.5	27.1	29.0	31.1	33.5	36.3	39.5
2.45	.650	23.5	24.8	26.4	28.1	30.0	32.2	34.7	37.5	40.8
2.52	.671	24.3	25.7	27.3	29.0	31.0	33.3	35.8	38.7	42.1
2.60	.691	25.1	26.5	28.2	30.0	32.0	34.3	36.9	39.9	43.3
2.68	.712	25.9	27.4	29.0	30.9	33.0	35.4	38.1	41.1	44.6
2.76	.733	26.7	28.2	29.9	31.9	34.0	36.5	39.2	42.3	45.9
2.83	.753	27.4	29.0	30.8	32.8	35.0	37.5	40.3	43.5	47.1
2.91	.774	28.2	29.9	31.7	33.7	36.0	38.6	41.4	44.7	48.4
2.99	.794	29.0	30.7	32.6	34.7	37.0	39.6	42.6	45.9	49.6
3.06	.814	29.8	31.6	33.5	35.6	38.0	40.7	43.7	47.1	50.8
3.14	.834	30.6	32.4	34.4	36.6	39.0	41.7	44.8	48.2	52.1
3.21	.854	31.4	33.3	35.3	37.5	40.0	42.8	45.9	49.4	53.3
3.29	.876	32.2	34.1	36.2	38.5	41.0	43.9	47.0	50.6	54.5
3.36	.894	33.1	35.0	37.1	39.4	42.0	44.9	48.1	51.7	55.7
3.44	.913	33.9	35.8	38.0	40.4	43.0	46.0	49.2	52.9	56.9
3.51	.933	34.7	36.7	38.9	41.3	44.0	47.0	50.3	54.0	58.1
3.58	.952	35.5	37.5	39.8	42.3	45.0	48.1	51.4	55.2	59.3
3.66	.971	36.3	38.4	40.7	43.2	46.0	49.1	52.5	56.3	60.4
3.73	.991	37.1	39.2	41.6	44.2	47.0	50.2	53.6	57.4	61.6
3.80	1.009	37.9	40.1	42.5	45.1	48.0	51.2	54.7	58.6	62.8

Fig. II-14

B. The Platinum Single Crystal Sample

1. Bulk Material

The samples used in this work were all cut from the same stock. This was a rod of ultra pure platinum single crystal 1/4 inch in diameter and 4 inches in length. The major heavy impurities present were determined by a spark source mass spectrometer. The results of this analysis are given in Table II-IV.

Table II-IV. Major impurities in the platinum sample used in LEED study

Impurity	(wt ppm)
Fe	30
Cr	25
Rh	15
Ag	< 30
Au	< 10
Ir	7
Pb	< 6
Si	4
Pd	2

2. Orientation and Cutting of Samples

The initial samples were cut using a diamond saw. Later on spark cutting techniques were used (with no noticeable difference in results). The large amount of material removed in lapping down to the final polish removed any effect of the method of cutting.

The thinner samples were difficult to work with as they were so easily deformed. The optimum thickness used was around 1.5 mm. The diamond saw enabled the desired face to be cut within 1°. The spark cutter lead to greater errors and a tolerance of ±2°.

Laue back diffraction x-ray patterns (Cu-Kα) were easily obtained from both the polished samples and the stock, but only after etch. These patterns were recorded by a Polaroid x-ray camera. The patterns were analyzed to determine the orientation of the exposed face. The LEED pattern is all cases agreed with that predicted from the three dimensional x-ray pattern.

3. Mechanical Polishing and Etching Techniques

Many techniques were tried to obtain an optically flat polished surface which was strain free. The final procedure which yielded excellent LEED patterns is as follows. The sample was polished and etched repeatedly (three times). Each succeeding final polish using 1/4 micron alumina powder seemed to introduce less damage.

Etching of the sample and holder was carried out using a diluted aqua regia solution (4 parts H_2O, 1 part HNO_3, 3 parts HCl) which was maintained at 100°C. More or less dilution led to etch pits. By using this technique immediately prior to mounting the sample in the chamber and evacuating, clear, bright diffraction patterns were obtained with small spot size (0.3°) without ion bombardment.

The degree of surface damage due to the surface preparation was estimated from the x-ray photographs. Microscopic examination always indicated etch pits as well as scratches over the entire surface.

For LEED experiments we have found that the macroscopic surface appearance of the sample is not necessarily a controlling feature on the

quality of the pattern. One sample was purposely left rough with etch pits (.1 mm deep) over the entire face. This sample gave an extremely clean pattern and exhibited the same features as other samples of the same orientation.

4. Mounting the Single Crystal Sample

Spot welding of platinum to platinum can damage the single crystal sample if precautions are not taken. To reduce the power required to form these welds, a .005 in diam wire of platinum was placed between the sample and holder. In this way the cross sectional area for flow of the welding current through the sample was reduced causing a hot spot. The weld thus occurred at this hot spot. These welds were extremely tough and were not the region of highest temperature in the system when the sample and holder were subsequently resistance heated in the chamber.

C. Selected Physical-Chemical Properties of Platinum and Platinum Oxide

1. The Structural Properties of Platinum

The crystal structure of platinum is face centered cubic with a lattice parameter of 3.9231 Å at 25°C.[11] The surface nets and interplanar spacings predicted from this bulk structure are listed in Table II-V.

Table II-V.

Face	111	110	100
Two dimensional unit cell	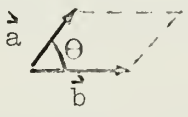	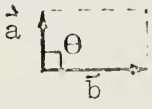	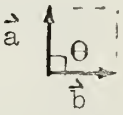
a	2.774Å	2.774Å	2.774Å
b	2.774Å	3.923Å	2.774Å
θ	60°	90°	90°
Planar spacing in z direction (perp. to the surface plane)	2.269Å	1.387Å	1.961Å
z spacing between equivalent planes	6.795Å	2.774Å	3.923Å
surface density of atoms per unit surface area	1.62×10^{15} atoms/cm^2	9.2×10^{14} atoms/cm^2	1.30×10^{15} atoms/cm^2

The difference between planar spacing and spacing between equivalent planes is important in specular intensity calculations. The spacing between equivalent planes can be compared to the spacing between planes for the 100 face to clarify the different values listed in the tables.

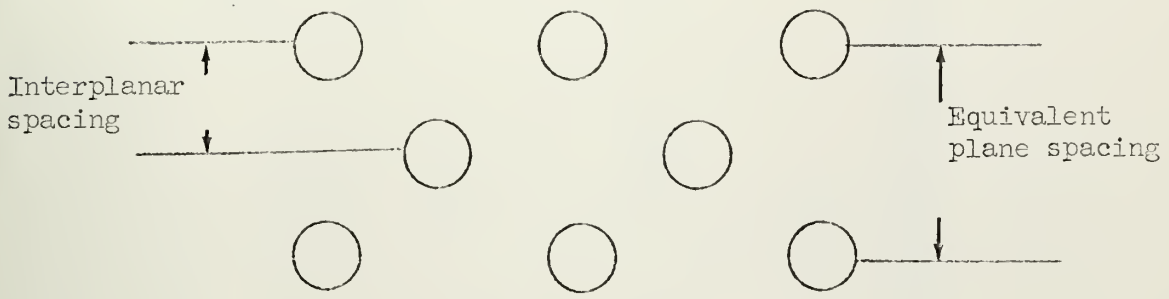

2. Heat of Evaporation and Free Energy Function of Platinum and Platinum Oxide

The thermodynamic properties of platinum and platinum oxide have been calculated only recently. The free energy functions are given in Table II-VI along with their references. These data then allow us to calculate the equilibrium partial pressures of platinum oxides as a function of oxygen pressure utilizing the following chemical equilibria

$$Pt_{(s)} + \frac{1}{2} O_{2(g)} \rightleftharpoons PtO_{(g)}$$

where

$$\exp - \frac{\Delta F}{RT} = \frac{[PtO]}{[O_2]^{1/2}}$$

and

$$Pt_{(s)} + O_2 (g) = PtO_{2(g)}$$

where

$$\exp - \frac{\Delta F}{RT} = \frac{[PtO_2]}{[O_2]}$$

Table II-VI. Free energy functions

Ref.		$-(F^\circ-H^\circ_{298})/T$ cal deg						$H^\circ_{298}-H^\circ_0$ kcal	ΔH°_{298} kcal
		298.15°K	500°K	1000°K	1500°K	2000°K	3000°K		
(12)	Pt(g)	45.96	46.68	49.17	51.00	52.35	-	1.572	135.2
(13)	PtO_2(g)	61.8	-	68.4	72.7	76.1	81.4	-	-
(12)	O_2(g)	49.01	49.83	52.78	55.19	57.15	-	2.075	0
(12)	O(g)	38.47	39.06	41.07	42.61	43.81	-	1.607	59.55
(14)	PtO(g)	61.32	62.22	65.49	68.19	70.14	73.92	2.126	-

For $PtO_2(g) = Pt(g) + 2O(g)$ $\Delta H^\circ_{298} = 213\pm5$ (13)

$PtO(g) = Pt(g) + O(g)$ $\Delta H^\circ_{298} \geq 93$ (14)

3. Equilibrium Partial Pressures

The partial pressures of Pt, PtO and PtO_2 of equilibrium partial pressures are given in Fig. II-14 for PO_2 = 1 atmosphere and in Fig. II-15 for $PO_2 = 5X10^{-7}$ torr.

The rate of removal of a surface under free evaporation can be given by [15]

$$\text{Rate} = P_{eq}\,\alpha\sqrt{\frac{1}{2\pi MRT}}$$

where, if the evaporation coefficient, α, is unity ($\alpha = 1$) the rate is at a maximum. M is the molecular weight of the vapor, R and T have their usual meaning. Calculation of the maximum rates of removal of platinum from P_{eq} indicates that approximately one monolayer of platinum would be removed per second if the total equilibrium pressure of platinum species would be $1X10^{-6}$ torr. This would occur in our system at oxygen pressures of $5X10^{-9}$ torr and a sample temperature of 1273°K (1000°C). We have observed that the damaged surfaces may be removed by a high temperature anneal in oxygen.

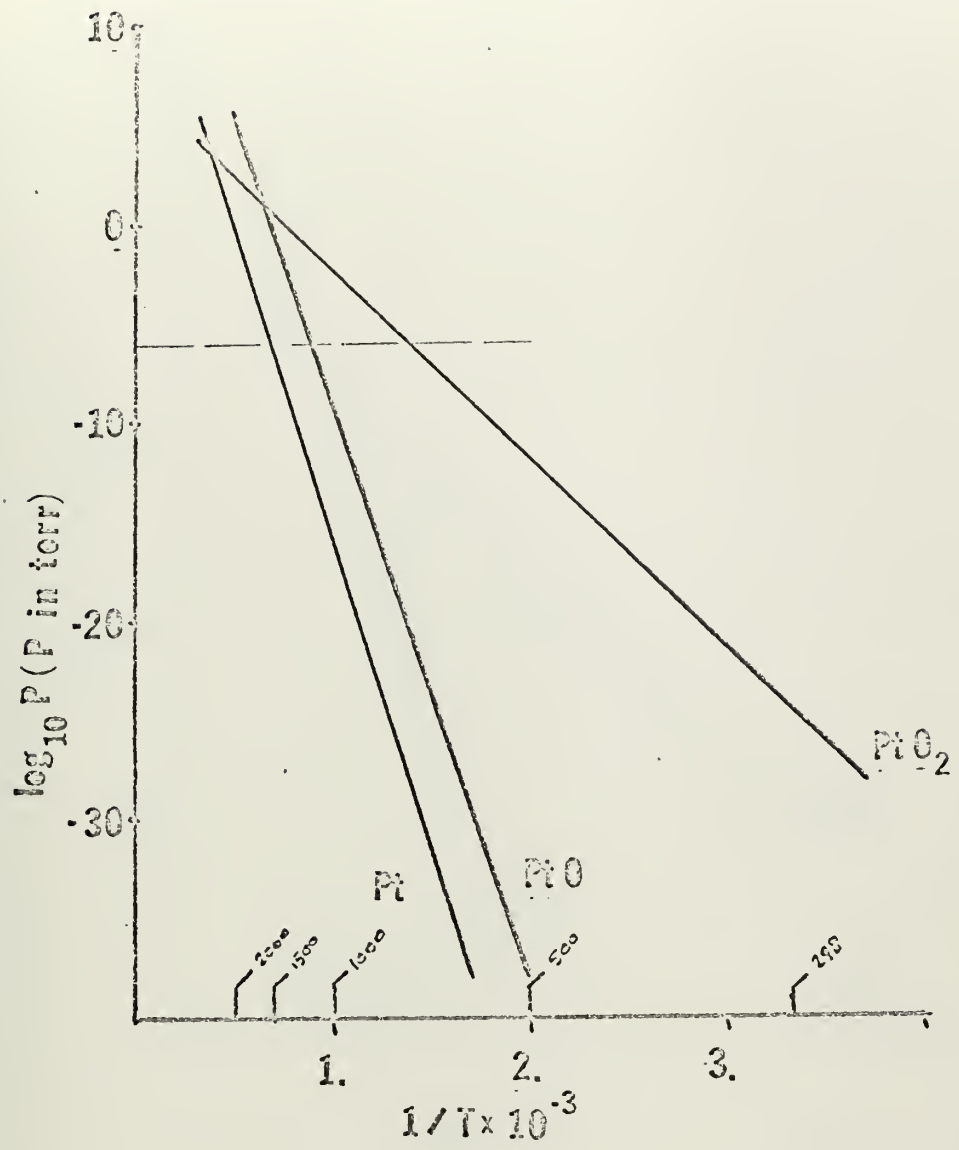

Fig. II-15. Equilibrium partial pressures of Pt, PtO, and PtO_2 for one atmosphere pressure of oxygen over solid platinum as a function of reciprocal Kelvin temperature. ($K^{\circ -1}$)

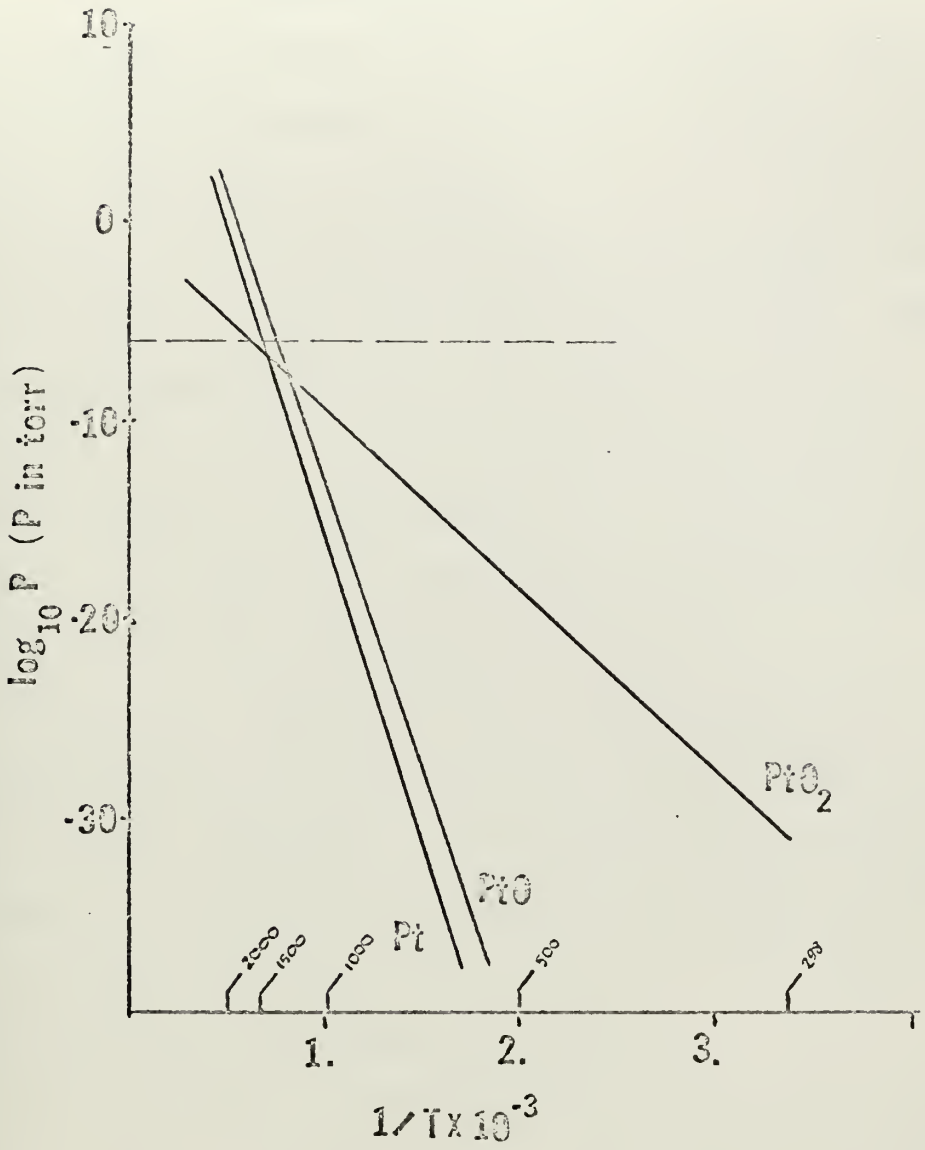

Fig. II-16. Equilibrium partial pressure of Pt, PtO, and PtO_2 for oxygen pressure of $5X10^{-7}$ torr over solid platinum as a function of reciprocal Kelvin temperature ($K^{\circ -1}$)

III. STRUCTURES ON THE (100), (111) and (110) FACES OF PLATINUM

A. General Considerations

The arrangement of atoms on the surface of a single crystal which coincides with the corresponding bulk structure is defined as "substrate structure." The presence of a substrate structure is verified by the characteristic diffraction features predicted from the bulk structure. Under well defined conditions extra spots may be formed.[16] These conditions are annealing in vacuum or the exposure to gasses.

The "extra" features observed as a result of the experimental conditions imposed on the sample indicate the existence of "surface structures." The locations of atoms within these surface structures are different from that in the "substrate structure."

The goal of LEED studies is to determine the cause of the structural rearrangement and to locate the exact position of atoms in the surface structure with respect to the substrate. If gas adsorption was necessary to cause the extra features then we would also like to determine if the gas atoms are part of the structure or they merely catalyze the surface rearrangement of metal atoms.

At the present these goals are only partially realized. "Extra" diffraction features have been observed as the experimental conditions varied, but the new location of the surface atoms could not be determined. However, the formation of these extra features under varying experimental conditions have allowed us to identify the cause of the appearance of these structures.

The specific details concerning the nature of the electron interaction with the surface have not as yet been resolved. The methods of

x-ray diffraction calculations cannot be applied to Low Energy Electron Diffraction experiments. The exact location of surface atoms in the surface structures cannot be calculated at the present. Furthermore, we cannot distinguish between diffraction by atoms of different elements, such as platinum and oxygen, since the atomic scattering factors of these elements for low energy electrons are not known.

The existence of diffraction spots leads to a definition of the size of the smallest unit mesh which describes the surface structure. We use the appearance of new diffraction features to monitor structural rearrangements.

B. Nomenclature

A vocabulary of surface crystallography has been established by E. A. Wood.[17] In this reference the definitions for surface structure and substrate structure are given in a manner similar to that stated earlier. A shorthand notation is developed for the indexing of surface structures and the designations of the unit mesh vectors. The unit mesh vectors in reciprocal space are designated as $\vec{a}^*$ and $\vec{b}^*$. Translations of $\vec{a}^*$ and $\vec{b}^*$ by the integers h and k generate the location of the spots within the diffraction patterns. The equation

$$\vec{r}_{hk}^* = h\vec{a}^* + k\vec{b}^* \qquad \text{(III-1)}$$

represents the pattern due to the substrate structure. The substrate unit mesh for the (100), (111), and (110) faces is given in Table II-5.

The established shorthand notation relates the existence of extra features to the substrate structure diffraction pattern. For example the symbols,

Pt (111) - (3 × 3)

denote a pattern which consists of a Pt(111) unit mesh in reciprocal space given by Eq. (III-1) upon which is superimposed another set of spots generated by the equation

$$\vec{r}^{*}_{h'k'} = \frac{h\vec{a}^{*}}{3} + \frac{k\vec{b}^{*}}{3} \quad . \qquad \text{(III-2)}$$

This notation does not mean that a solution of the location of the atoms in real space has been accomplished. The notation merely allows the re-creation of the position of extra spots in a diffraction pattern.

The existence of non-primitive unit meshes is allowed. The centered mesh is common in LEED patterns. To clarify, a pattern Pt(100)-C(2 × 2) would indicate a point at the $(\frac{1}{2}, \frac{1}{2})$ position as indexed by the substrate unit cell indices.

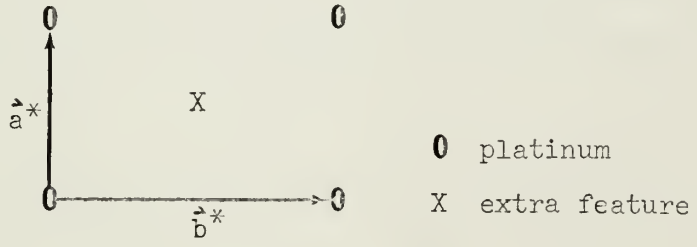

In designating the patterns which are due to the exposure of the crystal surface to a known gas, the chemical symbol of the gas is added to the shorthand notation. An example is,

$$\text{Pt(111)} - (2 \times 2)O_2 \qquad \text{(III-3)}$$

which indicates that the existence of these extra spots is dependent upon oxygen exposure. It does not imply however, that the new diffraction features are due to a periodic arrangement of oxygen molecules on the metal surface.

C. Definition of a Clean Surface

The designation in Eq. (III-3) is a brief description to part of the reproducibility requirements for the formation of a given pattern. From this notation one says that, if the platinum (111) face is exposed to a controlled flux of pure oxygen, one should expect the extra features indicated. The extra features may or may not be due to oxygen molecules or oxygen atoms, platinum or platinum oxides, carbon monoxide or other impurity oxides.

Impurities which are present in the substrate may also effect the formation of certain surface structures. Since LEED is sensitive to a monolayer of adatoms it is difficult to determine the concentration of impurities required for the formation of suspected patterns.

A "clean" surface can be defined as a surface of a crystal which has been purified by all known techniques, if not in contact with obvious sources of other impurities and by necessity is in an ultra-high vacuum system.

In studies of gas adsorption on metal surfaces the adsorbed species may diffuse into the bulk upon heating of the sample. This occurs in addition to the normally observed gas desorption process. The possibility of this bulk diffusion is often overlooked. The presence of dissolved gases in the bulk of the crystal can affect the properties of the gas-solid interaction and thus the reproducibility of the experiments. The prior history of a sample, especially concerning gas exposure and heating temperatures, must be considered in the interpretation of the experimental results.

D. The Effect of Domains

The electron beam covers approximately one square millimeter of the crystal surface. Within this area there are approximately 10^{13} surface atoms. Experience has shown that scanning the beam around the crystal face leads to a change in the intensity of "extra" diffraction features. In fact, many times different symmetries are present at different positions on the face and various patterns can be superimposed at intermediate positions of the electron beam.

It is apparent that the diffraction features are due to the periodic arrangement of atoms in surface domains. As long as the electron beam diameter is much larger than the domain size, the diffraction pattern will be the result of simultaneous diffraction by atoms in many domains. The symmetry of the exposed face may determine the possible number of equivalent orientations of domains.

E. Surface Structures

There are extra diffraction features which have appeared on the three different faces of platinum. These will be discussed separately for each face of single crystal platinum. First we shall describe the properties of those structures which formed by temperature annealing without exposure to gas. Then, we will be concerned with structures which are formed upon exposure to different gases.

1. The (100) Face of Platinum

a. Pt(100)-(5×1). The 100 face of platinum has a square reciprocal space unit mesh. The (5×1) pattern is superimposed upon the substrate structure along the principle axes which are the (011) and (0$\bar{1}$1) directions of the 3-dimensional unit cell. The assignment (5×1) is due to the 1/5 order spots which occur.

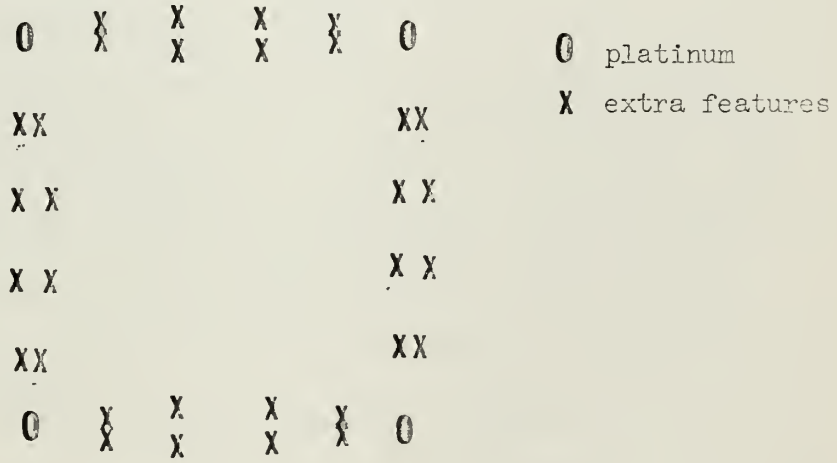

The doubling of the spots is apparent in all diffraction photos of the (5×1) and has been left out of the shorthand notation due to lack of appropriate symbols. The intensities of the extra order spots have been recorded (Fig. III-1) and can be equal or greater than the intensity of the principal spots. The relative values of these intensities are not as expected from simple kinematic models assuming the presence of ordered arrays of atoms or vacancies on the surface.

The pattern as drawn is really a superposition of two patterns rotated 90° to one another. One of these two orientations may be observed separately by careful positioning of the electron beam. This pattern has been formed repeatedly under "clean" conditions as defined earlier. On certain samples this was more difficult than on others. However, on no sample was the pattern unobtainable. Through the course of the work the pattern has been formed many times under varying conditions. The following short summary lists the experimental observations which could be used to verify the nature of the surface structure.

1) Kinetics of formation were measured by monitoring the rate of growth as a function of different temperatures (Fig. III-2). The initial rate of formation at each temperature was used to establish an estimate of the energy of activation with a value of 38 kcal/mole.

2) Under "clean conditions" the (5×1) appears to be stable in the temperature range of 300-500°C. At temperatures above 500°C the pattern will anneal away. In UHV the pattern can only be regenerated by heating after ion bombardment.

3) The pattern is faintly visible at 500°C and has been observed to disappear slowly upon cooling to room temperature in UHV.

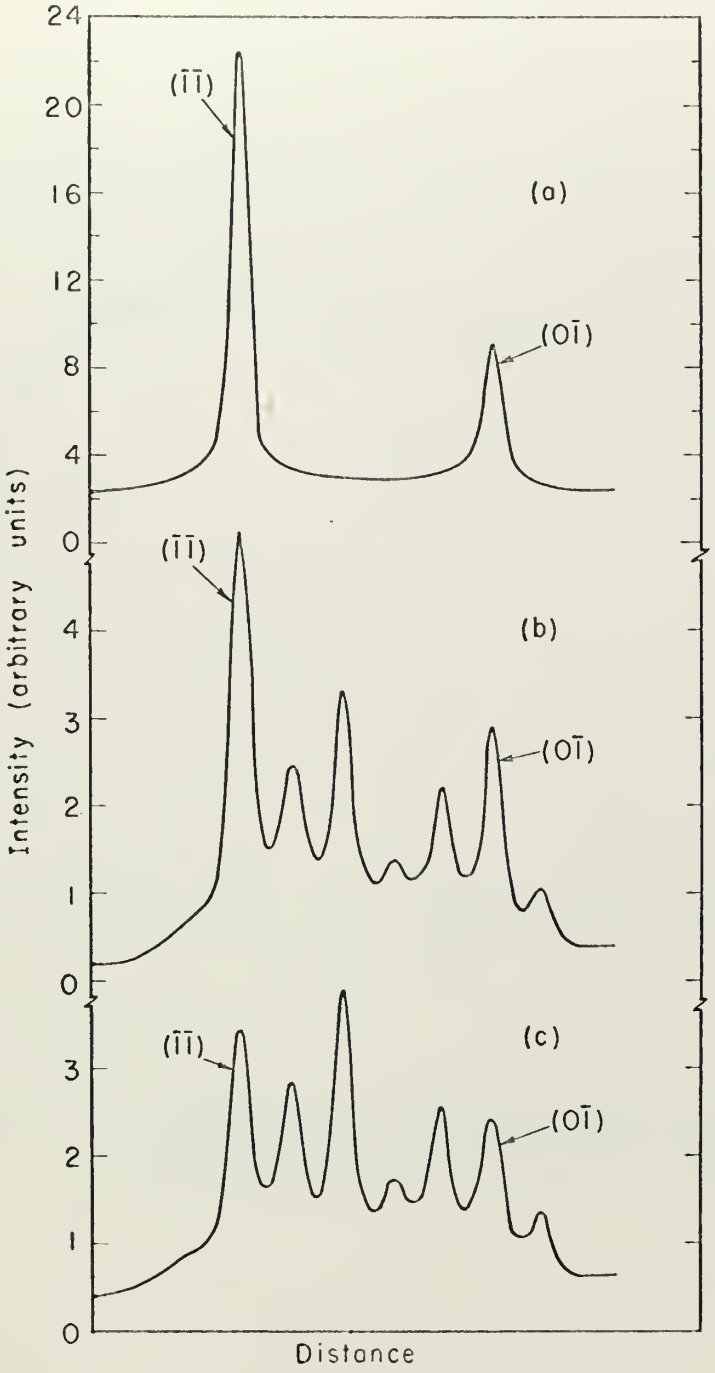

Fig. III-1. Intensity scan between $(\bar{1}\bar{1})$ and $(0\bar{1})$ platinum spots in order to show intensity of extra features for a) no 5X1, b) slight anneal, and c) longer anneal

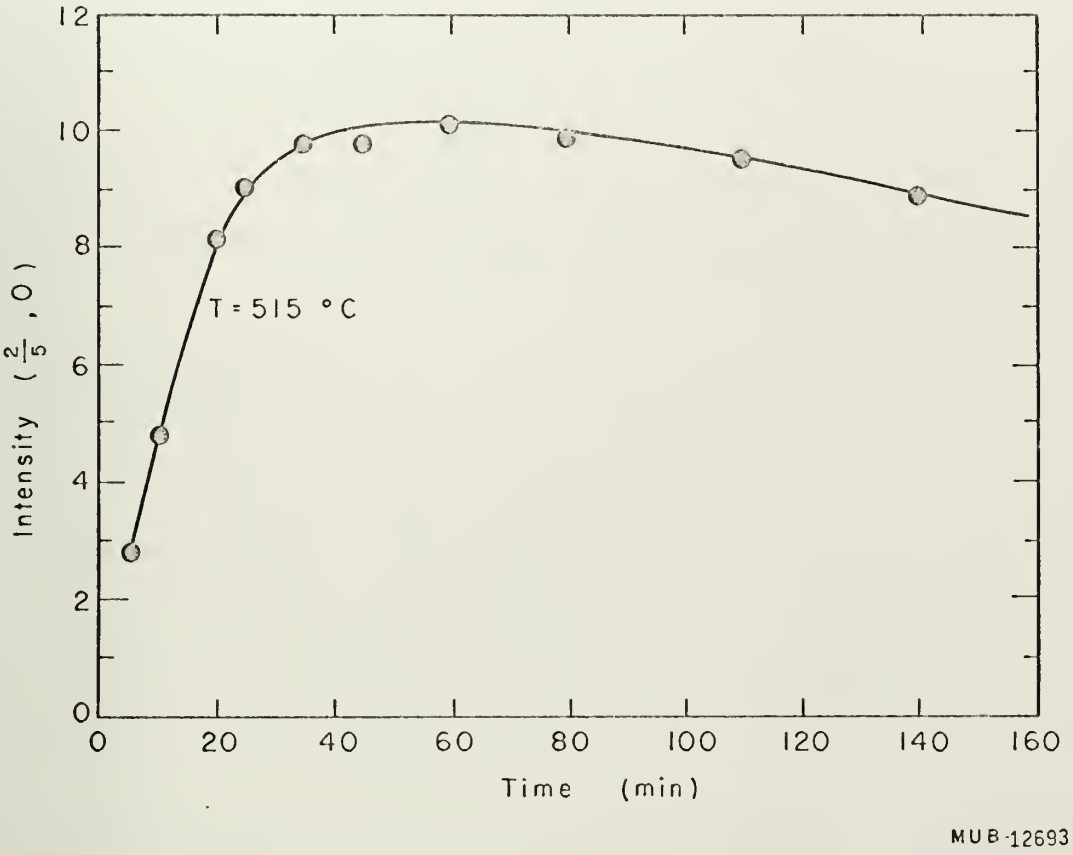

Fig. III-2. Intensity of one Pt(100)-(5X1) spot as a function of time at a temperature of 515°C during ultra-high vacuum anneal

4. The (5×1) pattern will disappear at room temperature in approximately 48 hours. If allowed to decay in this manner it can be regenerated by heating in the 300°-500°C range.

5. The (5×1) formed on many platinum (100) samples. On one sample a temperature gradient was required to form the pattern.

6. In all cases a clean Pt(100) structure was necessary as a starting point to form the (5×1). This clean substrate structure was then bombarded with xenon to prepare the surface for the formation of the (5×1).

b. Pt(100)-(2×1)

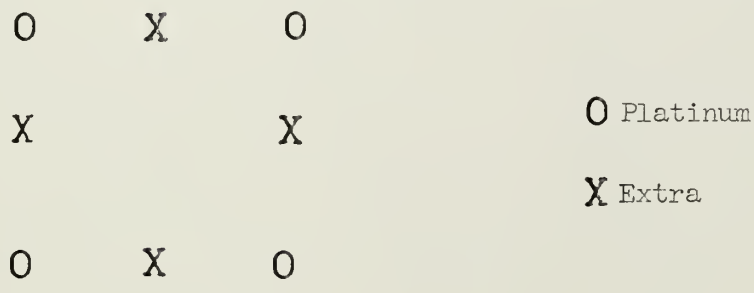

The assignment of this pattern to a set of superimposed perpendicular domains of (2×1) is due to the absence of the centered $(\frac{1}{2}, \frac{1}{2})$ spot. The characteristics of the (2×1) are less well defined than the (5×1). This pattern seems to be a precursor to the (5×1) but was not observed to coexist with the (5×1). In the initial stage of formation the extra order spots appeared as elongated spots, almost line segements. This would then coalesce into spots with further heating.

It was difficult to obtain the (2×1) since the (5×1) formed so readily at nearly the same temperature. This structure was not observed to form under oxygen treatment with conditions similar to that necessary for the (5×1).

c. Pt(100)-(5×1)O_2. The diffraction features of this pattern are the same as described in Sec. III-A. The addition of the oxygen symbol to the to the shorthand notation is due to the sensitivity of the rate of formation and the rate of decay of this pattern to oxygen pressure. When the (100) face is exposed to oxygen at 400°C which is within the range of stability of the (5×1) surface structure, the pattern formed in 120 seconds at a temperature of 400°C and a pressure of 5×10^{-7} torr O_2. If the sample is cooled to room temperature in the presence of oxygen the pattern disappears within seconds. If the (5×1) structure which can be maintained in vacuum at room temperatures for many hours is exposed to oxygen at room temperature, it decays within seconds. The rate of decay was measured and at $P_{O_2} = 8\times10^{-7}$ torr the pattern disappeared completely in 35 seconds at room temperature. If the oxygen pressure is reduced to below 1×10^{-8} torr the pattern remains for hours.

The rapid disappearance of this surface structure in the presence of oxygen explains why Tucker has not been able to observe its presence on the (100) face of platinum. Tucker cooled his samples from 400°C in a high pressure of oxygen ($P_{O_2} = 2\times10^{-6}$ torr). In our apparatus this treatment would cause the (5×1) to completely disappear in seconds.

d. Pt(100) C(2×2) CO

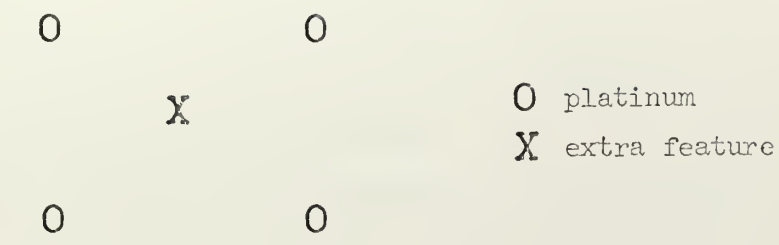

This pattern was the only new structure observed under controlled gas conditions. It was reproducible but only with difficulty due to the long exposure times required. The pattern formed at room temperature with CO (P_{CO} = 5×10^{-8} torr, time = 11 hours).

The pattern also formed at higher temperatures in O_2. This may be explained by the possible conversion of O_2 to CO in the metal gas manifold. We have not been able to verify this since we did not have the mass spectrometer operating for this series of oxygen experiments. It was observed that the presence of the (5×1) surface structure appeared to block the formation of the C(1×1). In similar manner the C(1×1) blocked the formation of the (5×1) structure.

e. Patterns of unknown origin. Near the completion of this work metallographic techniques had progressed to a state which allowed the observation of clean diffraction patterns after pump-down and bakeout without anneal or bombardment. Upon reaching this goal, certain "extra features" were observed which could be removed by annealing.

We attempted to reproduce these patterns at room temperature and elevated temperature by exposure to gases. Hydrogen, oxygen, nitrogen, carbon monoxide, ethylene, and ammonia were all used and none of these patterns could be regenerated. The patterns are interesting in that they indicate large unit meshes but do not demonstrate the doubling of spots which occurs with the Pt(100)-(5×1). They are recorded here in the hope that their very existence may illuminate future work.

Pt(100)-C(8×8) ?

O platinum
× extra feature

The Pt(100) sample had been etched and polished in the manner mentioned earlier in the crystal preparation section (II-B-3). The sample was washed in methanol, placed in the chamber in an argon atmosphere. The system was then immediately pumped down and baked for 8 hours at 250°C during which time the pressure fell to 5×10^{-8} torr. The sample was flashed immediately prior to bakeout to outgas and test the electrical connections. After the system cooled to room temperature and the optics were energized, the pattern was visible.

The pattern could be removed by flashing to 650°C and a mass spectrum was made during this heating. The predominate increase in background was contained in the m/e = 28 peak assumed to be CO. After this flashing the

pattern evolved to the Pt(100)-(2×1).

Pt 100 (2×1) elongated

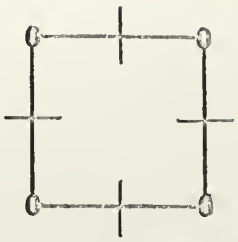

O Platinum

—— Extra feature

This pattern was formed after flashing the Pt 100 C(4×4)? to 650°C. There were continuous lines of intensity between the principle diffraction spots. A diffuse (2×1) the same as mentioned earlier appeared superimposed upon this pattern.

Pt (100)-(2×2) ?

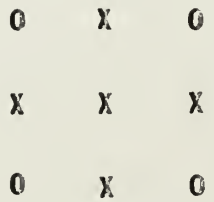

O Platinum

X Extra feature

A sample which was indicating a substrate structure diffraction pattern was let up to a predominately argon atmosphere, while the system was opened for approximately 20 minutes. Upon pumpdown and bakeout the Pt(100) (2×2) ? was formed. This pattern was easily removed by flashing the sample to a high temperature (T > 650°C).

Pt(100)-C(4×4) ?

O Platinum

X Extra feature

After a new sample had been prepared and placed in the chamber in a similar fashion to the Pt 100 (4×4) ? but this time the Pt 100-C(2×2) structure was formed.

f. Discussion of the (100) surface patterns. The (5×1) pattern is due to a surface structure which is created in "clean" surroundings, in ultra high vacuum by annealing after ion bombardment. This structure can also be created by heating in oxygen at 400°C and be destroyed by the presence of oxygen at room temperature. There are two possible diffraction mechanisms to be considered and each would lead to a different analysis of the structure causing the pattern. The unit cell has apparent dimension five times the bulk unit cell in one principal direction and is the same as the bulk dimension in the other. To give the required intensity a kinematic model would lead to a one or two vacancy surface structure. The high non-equilibrium concentration of vacancies at the surface is created by the ion bombardment treatment. Oxygen may also facilitate the creation of vacancies in the surface due to the free evaporation of PtO or PtO_2 as discussed earlier (Sec. II-C). Thus, the presence of oxygen could have the same effect as ion bombardment treatments in introducing surface vacancies which are necessary for the generation of the (5×1) pattern in ultra high vacuum. The inability to regenerate the pattern when heated to high temperatures would also be explained since the equilibrium concentrations of surface vacancies is reduced below that needed for the formation of these patterns.

However if multiple scattering is allowed then the Pt(100) surface diffraction pattern can be thought of as a source of multiple beams. In this case a new structure can be postulated which would explain the (5×1) pattern. This pattern would occur if a surface layer of some compound were formed with a spacing 5/6 or 5/4 the Pt spacing. In

these two cases the unit mesh projection on the surface plane would be either 1.15A or 1.73A. This would also require the same vacancies to exist as previously required unless the layer were thought to be composed of impurity atoms or molecules alone and out of registry with the lattice. The splitting of the diffraction beams may be due to the presence of anti-phase domains which occur in x-ray studies.[18]

This pattern will not be observed if the sample is cooled in oxygen. Experiments show that the pattern will disappear in oxygen in the time required for the sample to cool to room temperature.

The (5X1) surface structure is not unique to platinum and has been reported on gold.[19] This pattern has the same characteristic splitting as has been observed on Pt. These patterns are not unique to particular substrates but seem to be common to elements of the noble-metal, transition-metal family.

2. The (110) Face of Platinum

a. Pt(110) surface structures. Without oxygen pre-treatment there was no formation of distinct "extra" features in the diffraction pattern of the 110 face. Ion bombardments followed by annealing of the sample led to diffuse patterns with only faint hints of extra features. The sample preparation technique which worked so well for the (100) and (111) faces led to a much more disordered surface for the (110).

A higher temperature anneal in oxygen (7.4×10^{-4} torr seconds at 1200°C) caused a marked improvement in the diffraction intensity. No faceting of the surface was observed during this treatment. After this pre-treatment all of the observed patterns would form.

All of the patterns could be removed by xenon bombardment and formed by heating afterwards.

b. Pt(110)-(2×1). The 110 face of platinum is the only one of the three faces which were studied with an asymmetry which would make for example a (2×1) pattern different from a (1×2) pattern. The two non-equivalent 3D crystallographic directions which define the (110) surface unit mesh are the (001) direction and the $(1\bar{1}0)$ direction.

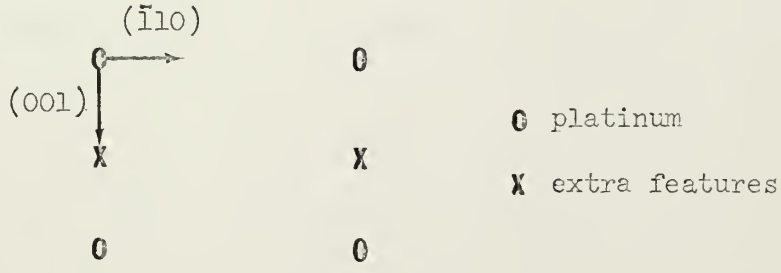

In this work (2×1) will refer to extra spots in the half positions along the (001) direction. This pattern formed by flashing the sample to high temperature (1300°C).

c. Pt(110)-(3×1)

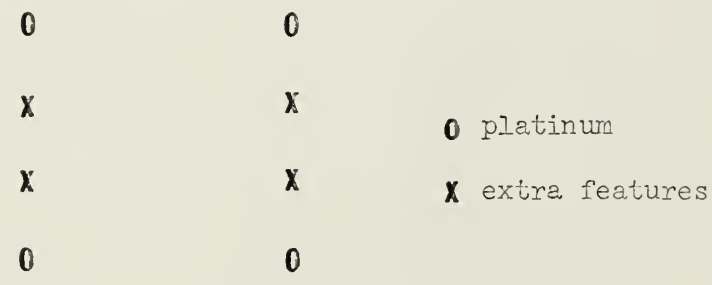

This pattern formed if the sample were flashed. A representative maximum temperature was 1380°C. The pattern was very distinct up to beam voltages as high as 450 volts. The (2×1) and (3×1) were observed to exist in separate domains after the flashing treatment.

d. Pt(110)-(4×1)

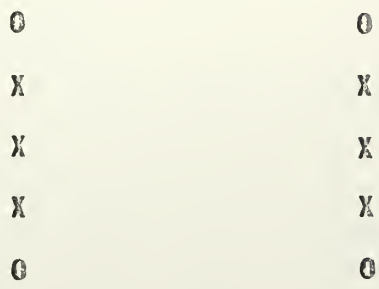

Only on the first flash after ion bombardment would this pattern form. Domains of this pattern could be found among the (3×1) and (2×1) domains.

e. Patterns of unknown origin

Pt(110)-(1×2) ?

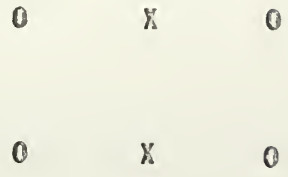

This pattern formed very faintly before the sample was pretreated in oxygen and also afterwards. This pattern disappeared with flashing.

Pt(110)-(1×3) ?

This pattern formed superimposed with the (3×1) after the sample was left in vacuum for 6 hours or more after the (3×1) was formed. Flashing caused the (1×3) to disappear but not the (3×1).

Pt(110)-C(2×2) ?

This pattern was observed alone and superimposed with the (2×1) and (1×2). The pattern would disappear when flashed in vacuum.

Pt(110)-(3×3) ?

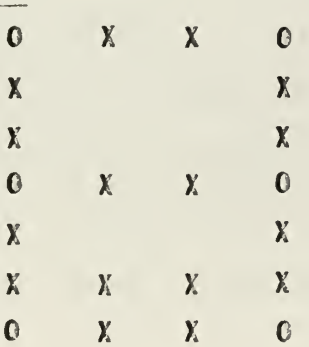

This pattern was formed as an intermediate in a flashing sequence. If the (2×1) were allowed to stand over night one flash to 1200°C would form this pattern. A second flash would remove the horizontal row spots leaving only the (3×1).

f. Discussion of Pt(110) clean surface structures. The necessary pre-treatment in oxygen used in this work makes it difficult to rule out the possibility that oxygen may play a role in the formation of these patterns. However, heating a developed (2×1) or (3×1) structure in hydrogen to 1200°C did not affect the pattern.

The patterns with multiple periodicity in the (001) crystallographic direction, for example (2×1)(3×1)(4×1) seemed to be created by high temperature anneal. The patterns multiply periodic in the ($\bar{1}$10) crystallographic direction, for example (1×2)(1×3), seemed to be created by long exposure to ambient gases in vacuum and destroyed by heating. Further discussion concerning the effect of gases will be covered later.

The (2×1) structure was also observed by Gjostein[19] in gold in vacuum. This was formed by vacuum anneal of the gold after ion bombardment.

g. Pt(110) gas studies. If the Pt(100)-(2×1) or (3×1) patterns which had been formed by vacuum anneal were exposed at room temperature to oxygen or carbon monoxide the extra spots immediately disappeared. The rate of decay appeared to be a function of pressure. Due to the difficulty in making intensity measurements during oxygen exposure, kinetic data were attempted with carbon monoxide.

The (2×1) structure was formed by flashing the sample ($T > 1300°C$) and the well developed (2×1) was present when the sample cooled. Chamber pressure remained less than 5×10^{-9} torr during this heating. CO was admitted to a constant pressure which was varied for each run. Upon the

admission of the gas the intensity of the extra spots dropped. The initial rate of change of intensity compared to the maximum value of the intensity was a function of the pressure of CO. The parameter

$$\frac{d\,(I_{(t)}/I_0)}{dt} \quad (sec^{-1})$$

is the measure of this initial rate. This parameter is plotted in Fig. III-3 as a function of pressure.

The spot disappeared entirely in 10 seconds at a pressure of 2×10^{-7} torr carbon monoxide. This is a rather remarkable result as there appears to be no kinetics and the reaction probability of a gas incident upon the surface at time T = 0 is 1.0. To determine if this effect may be due to gas impact phenomena, the experiment was repeated with N_2. The nitrogen had no effect upon the pattern and there was no intensity decrease. It should be noted that the extremely rapid disappearance of the Pt(100)-(5×1) in oxygen at room temperature must be due to a similar reaction mechanism.

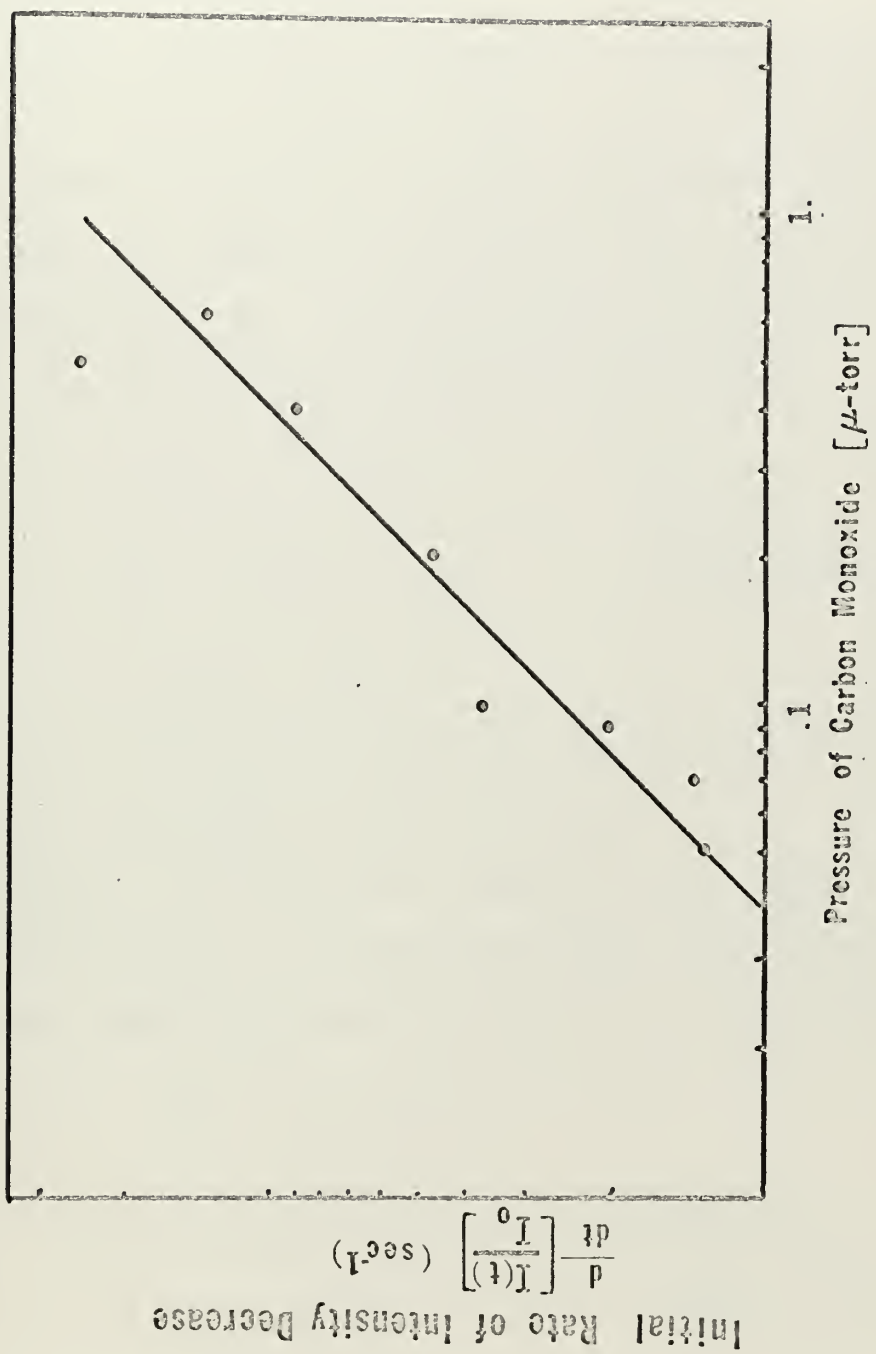

Fig. III-3. Platinum (110)-(2X1) surface structure room temperature rate of delay as a function of carbon monoxide pressure

3. The (111) Face of Platinum

On the Pt(111) face no surface structures were observed which were reproducible at will from sample to sample. The patterns reported were, however, distinct and clearly visible.

a. Pt(111)-(2×2) ? This pattern was formed by long high temperature anneal in ultra high vacuum (T = 700°C for 75 hours or more). It has been assigned to a clean structure. The length of anneal, however, makes it possible that its formation be effected by the presence of some of the more reactive residual gases (H_2O, CO, O_2). The pressure was low during anneal $P = 5\times10^{-9}$ torr. The structure is stable at high temperature

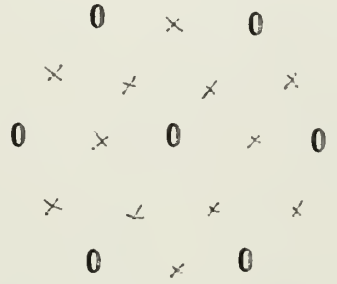

O Platinum

× Extra features

This structure was reproducible on one sample but could not be reformed after the sample was removed, etched and replaced.

b. Pt(111)-(3×3) ? This pattern was formed in similar manner to that above. The (2×2) appeared to be a precursor to the (3×3). Longer heating times or higher temperatures led to the formation of the (3×3) from the (2×2).

O Platinum

× Extra features

c. Pt(111)-(2×2)-O_2

Platinum

Extra features

This pattern was formed by a room temperature exposure of the sample to oxygen at a pressure of $P_{O_2} = 5\times10^{-8}$ torr for 32 minutes. The ion gauge was turned off during the first part of this experiment and had no effect upon the pattern when turned on. It was proposed by Tucker that the hot tungsten filament of the ionization gauge might be responsible for generating carbon monoxide which would destroy the O_2 pattern. After the pattern was formed and became clearly visible the sample was flashed to 1100°C. The pattern disappeared completely and an O_2 (m/e = 32) spectrum in the mass spectrometer indicated two desorption peaks at 455°C and 658°C. The sample was ion-bombarded to generate the standard starting condition but the (2×2) pattern never reformed. All types of conditions were imposed upon the sample but the pattern could not be duplicated.

d. Pt(111)-Hydrogen, oxygen, nitrogen, methane ethylene and ammonia. Immediately after the Pt(111)-(2×2)O_2 study listed above was completed, the Pt(111) surface was exposed to many different gases. The mass spectrometer was used in most of these studies.

The gases used were O_2, H_2, N_2, CH_4, C_2H_4, and NH_3. The presence of these gases did not seem to give rise to "extra" diffraction features. The exposures were approximately 50 micro torr sec. The experiments were carried out both at room temperature and at elevated temperatures. Except for oxygen exposure of an unannealed sample (described above) no

effect upon the diffraction patterns were observed, either in overall intensity or in the formation of extra peaks. The specular intensities as a function of beam voltage showed no change due to gas coverage.

There were no extra spots formed with the exposure of a freshly ion bombarded surface to oxygen. However there was a dramatic decrease in the intensity of the entire pattern when the unannealed surface was exposed with exposure to oxygen. If a freshly bombarded surface was annealed first then there was no decrease in intensity due to oxygen exposure. The results of this experiment are given in Fig. III-2. These data have been normalized to account for any change in incident beam intensity.

This figure (III-4) indicates that a layer of oxygen either does not adsorb on an annealed platinum (111) surface or that a layer of oxygen does not attentuate the electron beam scattering. Flashing experiments indicated that oxygen was in fact adsorbed on the surface in all of these cases. The same desorption peaks as observed for the (2×2) O_2 pattern were observed in all of these cases where no extra spots were formed. The mechanism of interaction is unknown but apparently the oxygen catalyzes the motion of a platinum atom out of an ordered position if the surface has already been disordered by previous ion bombardment. If the surface is ordered (long anneal) then oxygen has little effect upon the arrangement of platinum surface atoms.

4. High Temperature Ring Structures

On all faces of platinum a high temperature anneal ($T > 800°C$) leads to the formation of a ring structure. Upon initial formation, the rings are not complete circles and exhibit segments which have 12 fold rotational symmetry. Further heating at the same temperature, or a higher temperature

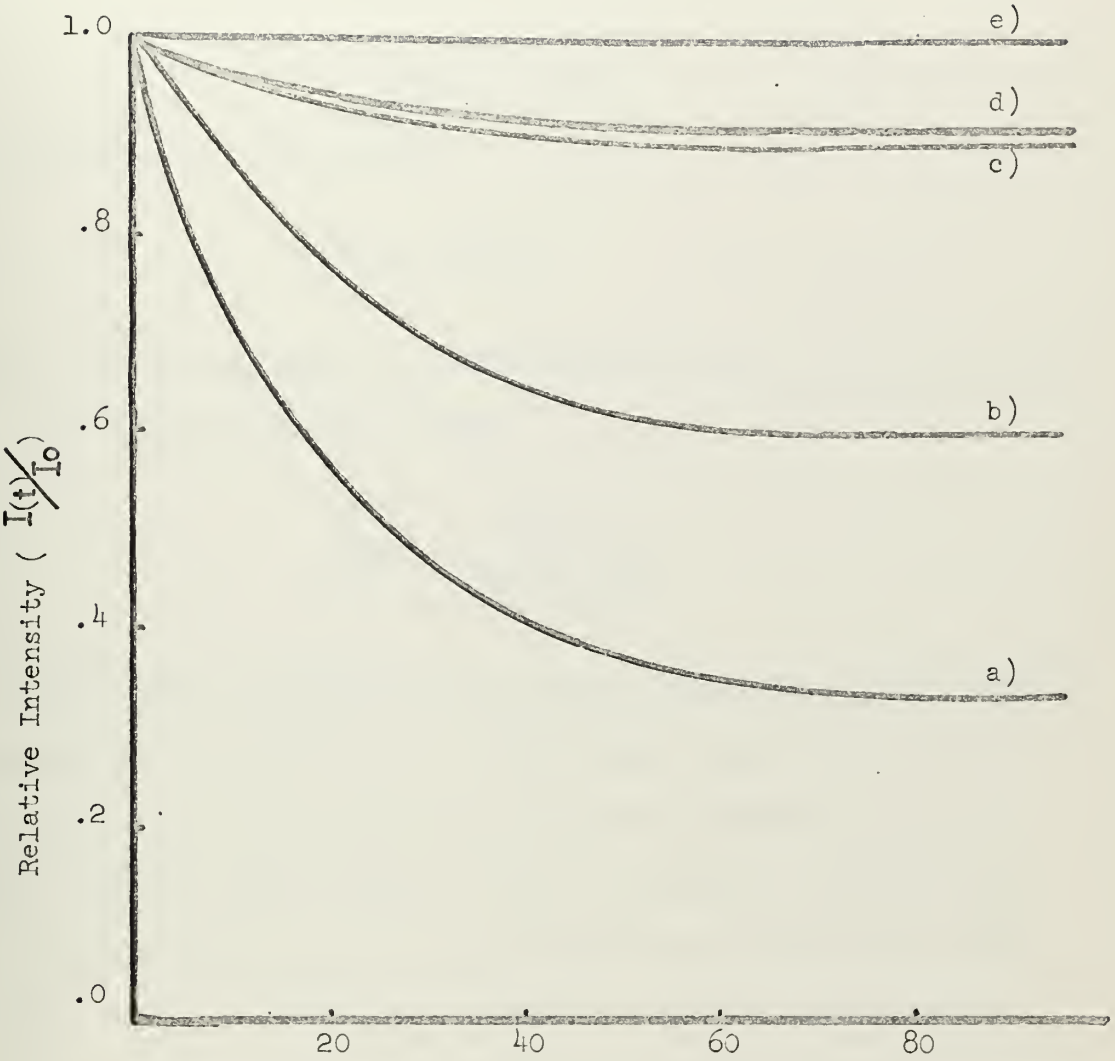

a)No anneal after bombardment
b)No anneal after bombardment
c)Anneal after bombardment 650°C for 17 minutes
d)Anneal after bombardment 500°C for 10 minutes
e)Anneal after bombardment 900°C for 52 hours

Fig.III-4. Effect of oxygen exposure on Pt in specular reflection at 58 electron volts

heating causes the ring segments to coalesce into complete circles.

The rings exhibit diffraction features like all the other diffraction patterns. This can be shown by the fact that the diffraction equation is satisfied for all eV:

$$\lambda = d_{ring} \sin(\theta_{ring})$$

If we calculate λ by the equation

$$\lambda = d_{is} \sin(\theta_{is})$$

where d_{is} is the real space inter-row spacing leading to the first order spot. We can derive the relationship

$$\frac{d_{ring}}{d_{is}} = \frac{\sin\theta\,(is)}{\sin\theta\,(ring)}$$

This relationship is independent of electron beam voltage. The results of the experimental determination of this ratio for the three faces of Pt and for the second and third rings are given in Table III-1.

The nearest neighbor distance (d_{nn}) in platinum is (d_{is}) for the (100) and (110) faces but not for the (111) face. For the (111) face $d_{is} = \frac{\sqrt{3}}{2} d_{nn}$. The data are corrected so that the three faces are all referred to as d_{nn} and these results are given in the second column of Table III-1.

The ring formed on the face of every sample studied. However on the (110) face which was pretreated in oxygen the ring would not form until after the surface was ion bombarded regardless of the temperature of annealing. The ring then disappeared upon flashing to 1250°C. It reformed after a week at room temperature in vacuum and was again removed

Table (III-1). The Ratio of the Lattice Parameters $d_{\odot}/d_{is}$ for the Different Sets of Rings on the (100), (111) and (110) Substrates of Platinum[a]

		$d_{\odot}/d_{is}$ (Experimental)	$d_{\odot}/d_{is}$ (Corrected)
Pt (100)	first	0.75 ± 0.03	0.87 ± 0.03
	second	0.43 ± 0.03	0.50 ± 0.03
	third	0.41 ± 0.03	0.47 ± 0.03
Pt (111)	first	0.89 ± 0.03	0.89 ± 0.03
	second	0.51 ± 0.03	0.51 ± 0.03
Pt (110)	first	0.78 ± 0.03	0.90 ± 0.03

[a] $d_{\odot}$ is the apparent lattice parameter which can be assigned to a diffraction ring and d_{is} is the interplanar distance in the substrate.

by flashing. This was the only time that the ring structure's characteristics were different. In all other cases the ring structure formed irreversibly and could only be removed by ion bombardment.

The ring has been observed on gold[19] as well as platinum. It appears that in both cases, the features are due to some surface structure which is out of registry with the lattice. The ring diffraction pattern becomes more dominant with heating and is extremely unreactive, i.e., could not be removed by heating (1000°C) in reactive gases (oxygen, hydrogen).

F. Conclusions

The platinum surfaces show the existence of reproducible ordered and disordered surface structures. The ordered structures have a periodicity which indicates that the surface unit mesh is an integral multiple of the bulk structure. The patterns of the ordered structures in general require some pretreatment to allow their formation. This treatment can either be ion bombardment and anneal or gas exposure to a hot sample.

These structures are much less sensitive to exposure to oxygen and carbon monoxide at room temperature than that observed for nickel[20] or palladium.[21] However, the rate of formation of some of the surface structures at elevated temperatures or rates of decay at room temperature are very sensitive to oxygen or carbon monoxide partial pressures. Therefore, oxygen or carbon monoxide can either partake in or catalyze the surface reaction which causes the extra spots. The presence of a small concentration of oxygen and hydrogen dissolved in platinum is also indicated by the sensitivity of the formation of some of the patterns to the prior thermal history of the sample.

The ambient background has been shown to have an effect upon these diffraction patterns. Flashing of the sample to high temperatures was found to be sufficient to remove the diffraction spots due to this mechanism.

The effect of amorphous layers has been observed on the (111) face when a disordered face was exposed to oxygen. A high temperature anneal after bombardment completely removed any effect of this type of oxygen adsorption.

These patterns differ from the earlier platinum work[3] in that they cover an entirely different temperature range. The temperature ranges of stability of the observed surface structures as reported in this work (400-1200°C) are very large compared with that reported in the earlier work (~ 80°C). New patterns have been observed to exist which could not have been observed if the sample had been allowed to cool under a gas pressure instead of high vacuum. There is a correlation between the properties of certain patterns, for example, Pt(100)-(5×1) and Pt(110)-(2×1).

The ring-like diffraction patterns indicate that the surface forms an irreversible disordered layer when heated to high temperature in vacuum. This layer is stable, unreactive and in most cases removable only by ion bombardment.

IV. ANALYSIS OF EXPERIMENTAL INTENSITY DATA

A. General Considerations

In this work two different types of intensity data were recorded. We have monitored the intensity of the specular (00)-reflection as a function of a) wavelength (beam voltage) and of b) temperature (Debye-Waller factor. The specular (00)-reflection was chosen for recording because it is most sensitive to the transition from two-dimensional diffraction to three-dimensional diffraction. The effect of lower planes on the scattered intensity is seen most dramatically at small angles of incidence. The specular intensity in the only spot in the diffraction pattern which does not change its position on the screen as the beam voltage is changed. To achieve this positional stability of the specular intensity (00-reflection) all electrostatic and magnetic fields must be removed from the diffraction region. This is accomplished by electrostatic screening, grounding, and trimming magnets. To interpret this data we use an optical diffraction model and the working equations based on this model are derived in Appendix A and B. The results of this derivation then are used to fit the experimental results.

The theoretical analysis of LEED beam intensities is a subject of great interest at present. The recent dynamical calculations of McRae,[22] Bauer,[23] and Heine[24] are only the precursors to a new and broader application of this more general theoretical approach to low energy electron diffraction problems. The dynamical scattering calculation considers the interaction of the electron wave with the crystal lattice in which no single scattering event can be considered independent of the others.

In this work we use a "pseudo-kinematical" approach to the interpretation

of the data. Our model takes into acout only those scattering contributions, in calculating the scattering amplitude and the intensity, which are necessary to obtain agreement with the experimental results. This is done for the sake of computational feasibility and physical insight.

B. Beam Voltage Dependence of the Specular Intensity

The recording of the specular intensity (00 reflection) as a function of beam voltage (wavelength) has been accomplished for all three faces of platinum which were studied. Representative curves for the (100) face have been chosen to demonstrate the changes in the intensity as a function of different variables because of the greater quantity of data acquired for this face. The time required to complete one recording (5 minutes) makes kinetic studies by this method difficult.

1. Comparison of the Specular Intensity Curves for the (100), (110), (111) Faces of Platinum. The specular intensity as a function of beam voltage has been recorded for the 3 faces of platinum studied. The angle of diffraction is shown in Table IV-1 for the respective face. These same three curves are plotted separately in Section C and compared with calculated values. The recordings show the extreme differences that exist in the specular intensities scattered by the different crystal faces.

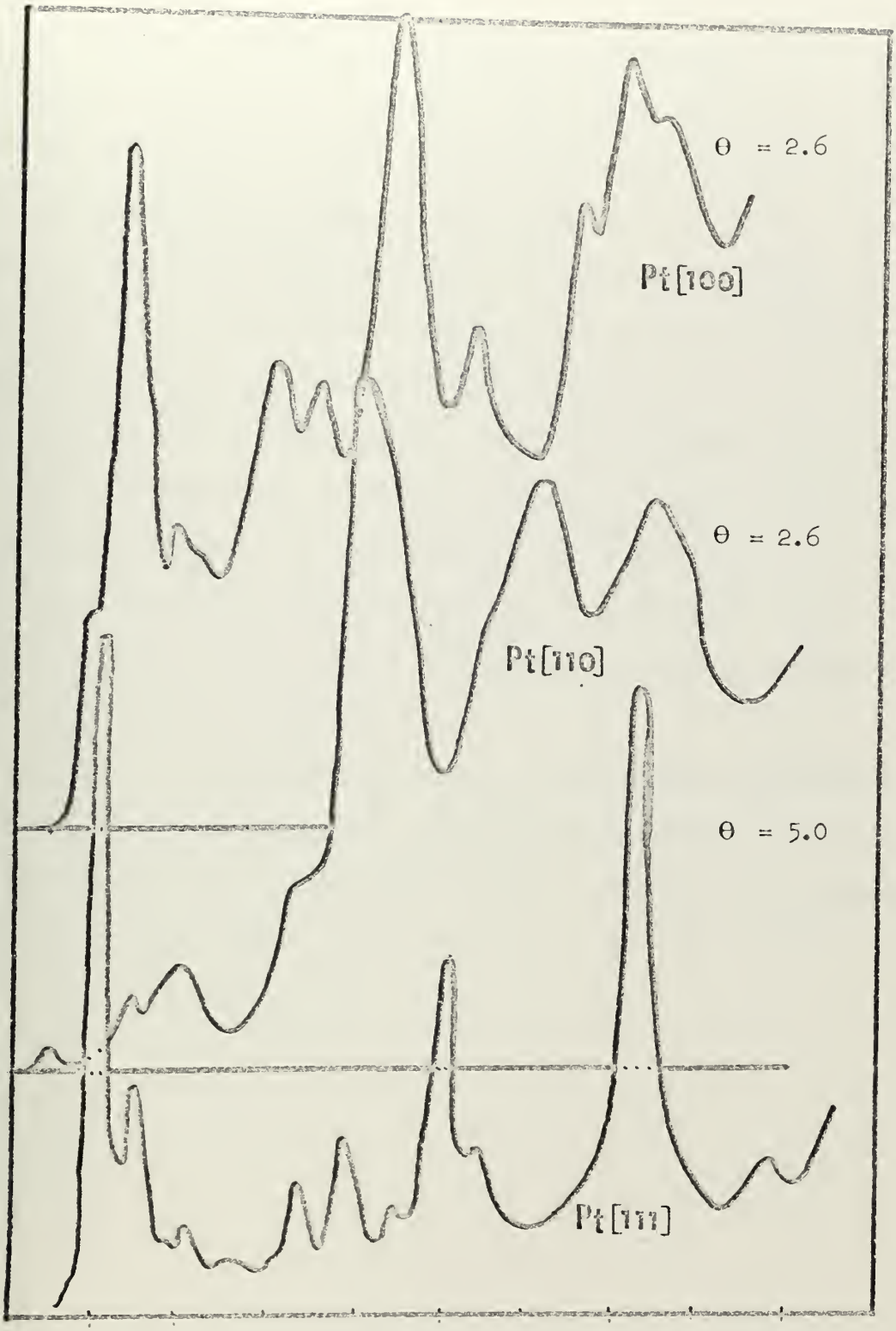

Fig. IV-1. Specular intensity as a function of beam voltage for the (100), (110) and (111) faces

2. Effect of Temperature Upon Specular Reflections. The recording of specular intensity as a function of temperature posed many experimental problems. The intensity which is back reflected varies as the beam is moved along the crystal surface. The heating current induces a motion into the beam which interferes with the measurement. A sample was prepared which gave uniform intensities independent of the position of the electron beam on the crystal face and the results plotted in Fig. IV-2 are from that sample. The data were taken at the high temperature (618°K) first and then at decreasing temperatures. The loss of intensity ascribed to the Debye-Waller effect is seen clearly. The weaker peaks at 100 eV and 350 eV are completely washed out while the stronger peaks continue to dominate. These recordings also were made on an angle of incidence of 2.6°.

There is no discernable shift in the beam voltages where maxima occur due to thermal expansion. This is to be expected as the published thermal expansion for platinum would predict a change of less than one volt for this temperature range.

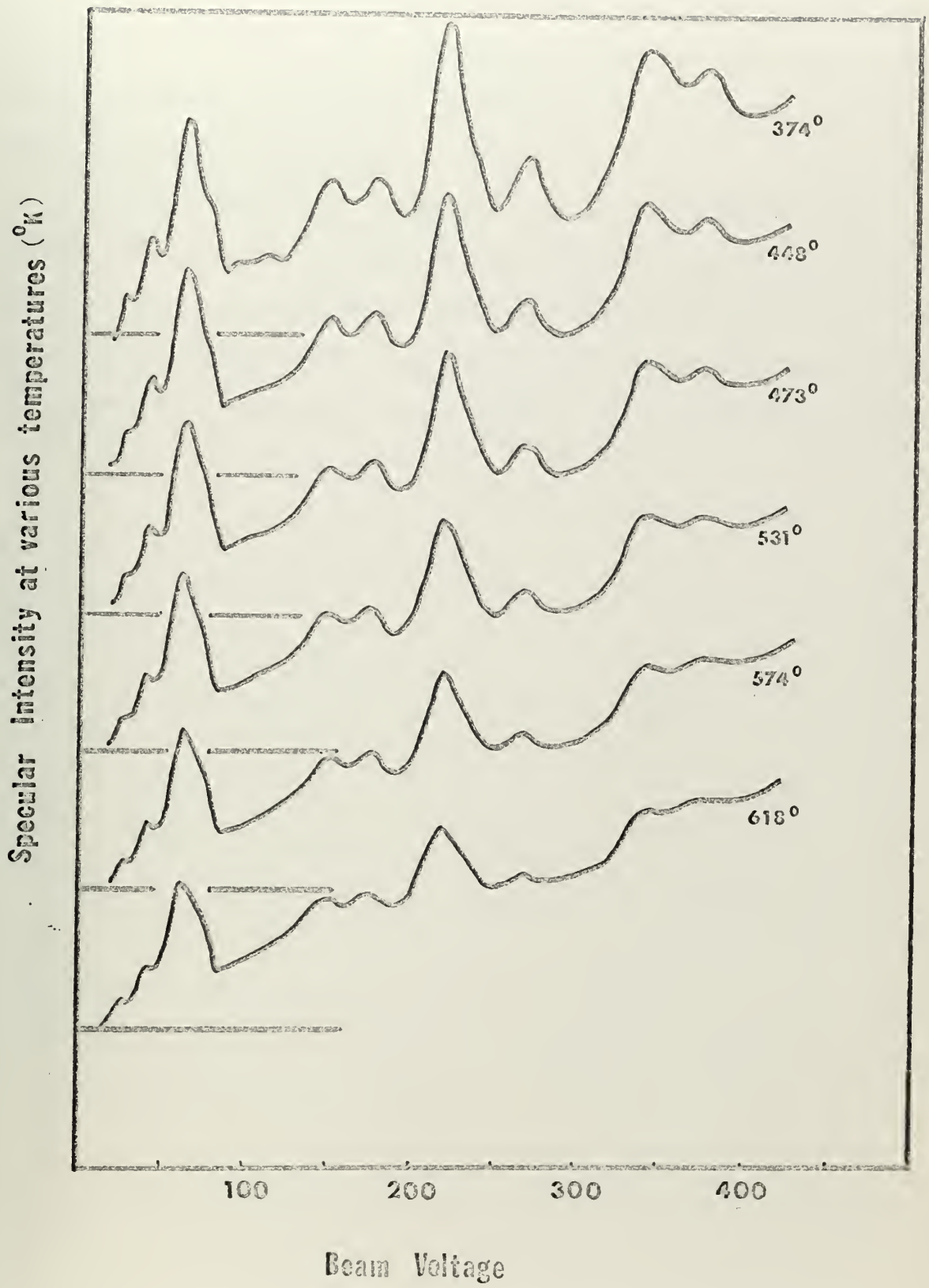

Fig. IV-2. Specular intensity as a function of beam voltage for the (100) face at different sample temperatures

3. Specular Intensity Compared to Background Intensity. In Figure IV-3 the specular intensity of the (100) face at an angle of incidence of 2.6° is shown. The background recording was made under identical conditions merely by rotating the specular reflection off of the phosphor screen and into the collimator tube ($\theta = 0°$).

The maxima observed in the background spectra at 65 eV is not an optical reflection from the specular spot but is a property of the background. However, this maxima is centered symmetrically around the specular reflection and demonstrates the properties of thermal diffuse scattering.[25] The background intensity is observed to rise with increasing beam voltage.

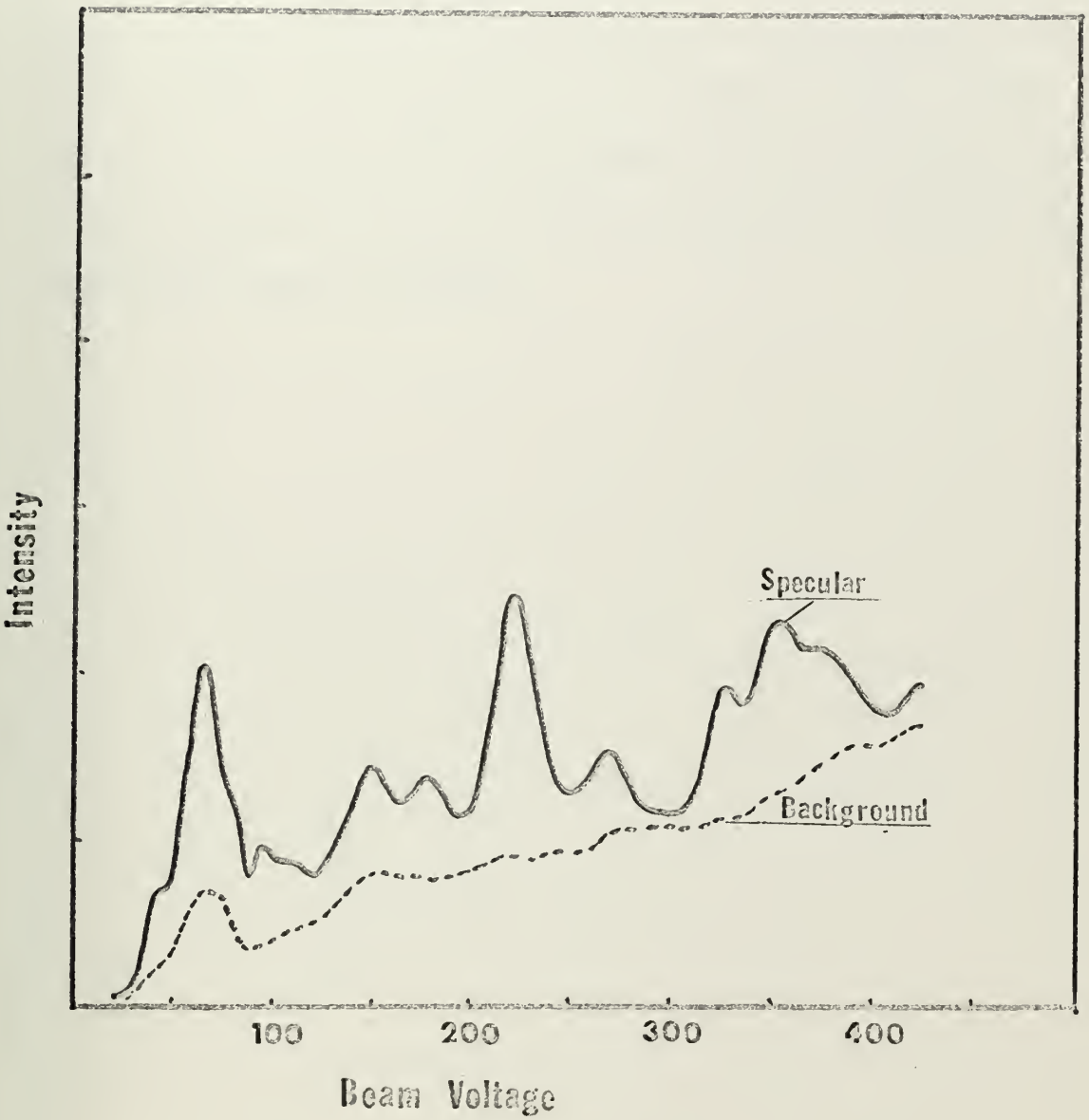

Fig. IV-3. Specular intensity as a function of beam voltage compared to background intensity. Diffraction angle = 5°

4. Reproducibility of Specular Intensity Measurements. As more and more data were accumulated certain features of the specular intensity showed differing properties, yet the measurements were made using "clean" surfaces. The disagreement in curves 1 and 2 of Fig. IV-4 between 300 and 400 volts cannot be explained at present. Curve 2 was made after curve 1 and the only differing condition was that the sample had been heated to 618°C in UHV between the two recordings. Similar effects have been noted on Pd by Park.[21] It is apparent that the characterization of a surface requires not only the existence of spots in the pattern but a reproducible specular intensity.

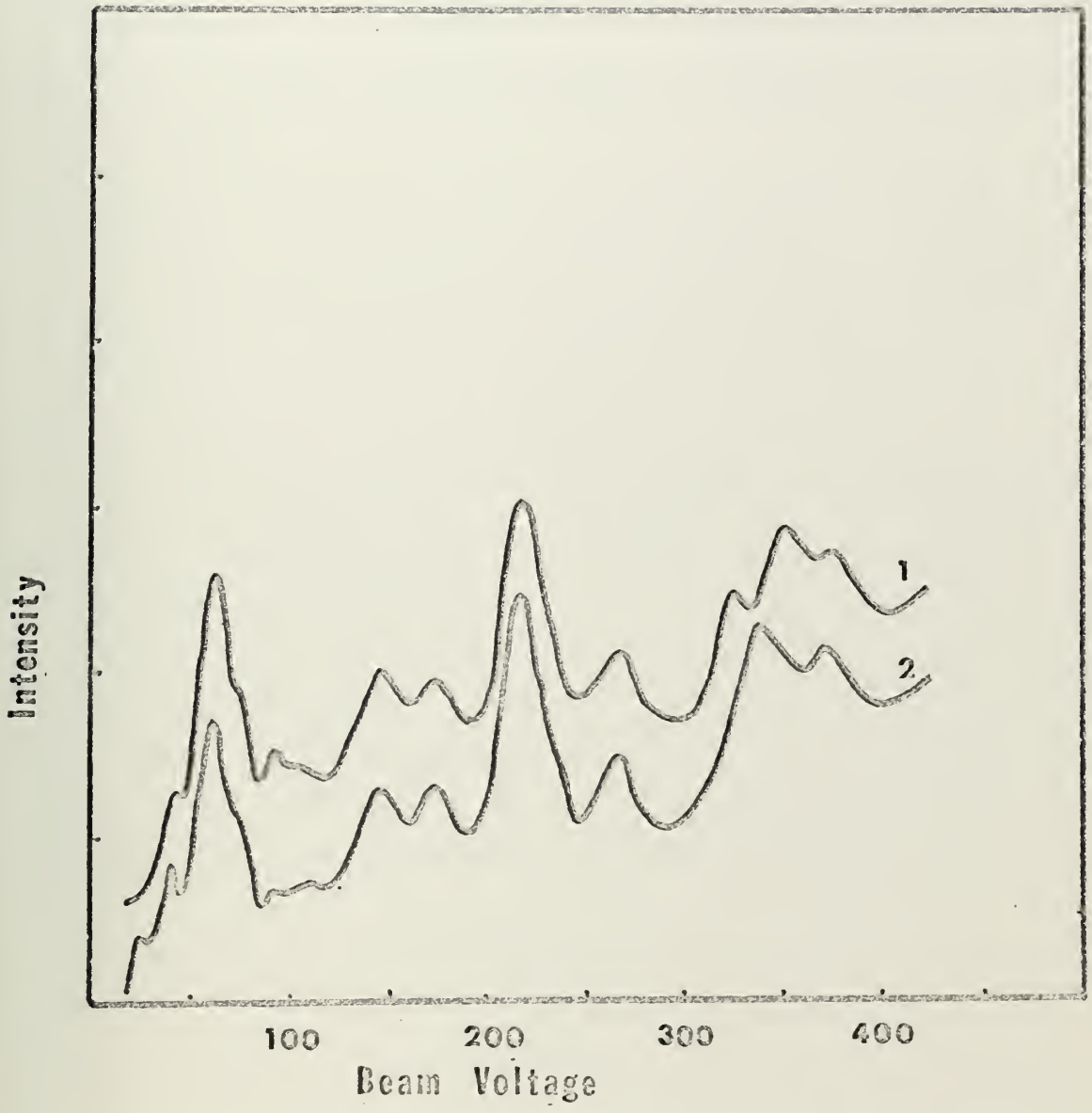

Fig. IV-4. Specular intensity of Pt(100) face as a function of beam voltage. 1) in UHU before flashing, 2) in UHU after heating to 618°C

5. Other Observations. There was no change observed in the (100) specular intensity recordings during deliberate exposure at room temperature to CO and O_2. No extra spots were formed during this treatment. This was done to attempt to correlate the loss of fractional order diffraction spot intensities observed on tungsten by May and Germer[26] to those observed on platinum. No similar effect was noted on platinum.

The existence of extra diffraction features, notably the Pt(100)-(5×1) and Pt ring structures did not introduce major changes in the specular intensity curves.

C. Comparison of Experiment with Pseudo-Kinematical Theory

The equation derived in Appendix A for the specular intensity scattered by equivalent set of planes (A-4) as a function of beam voltage has been applied to all three faces of platinum. These curves have been observed experimentally and the calculations were done using parameters which as close as possible duplicate the experimental condition. The incident beam intensity J_0 is given by the experimentally determined relationship

$$J_0 \alpha 2(eV) + 0.170\ (eV)^2$$

which takes into account the change of the emission current as a function of beam voltage. To allow for the beam voltage dependence of the penetration, the amplitude transmission factor T was given by the relationship

$$T^2_{(eV)} = T^2_0 + SxeV$$

in which S is the change in T^2 due to the change in voltage and T_0 was arbitrarily set to zero so that there is no penetration at zero voltage.

Table IV-1 gives the equation and the parameters used in these calculations for each of the three faces. In Fig. IV-5, IV-6, and IV-7 we have plotted the experimental and calculated curves for the (100), (110), and (111) faces. The calculated curves give a good fit to the experimental data predicting the position of the observed diffraction maxima.

The magnitude of the intensity maxima, however, cannot be calculated accurately by the pseudo-kinematical theory. If $(f_0)^2$ could be a rapidly fluctuating quantity then this parameter could explain some of the discrepancy.

Table IV-1

$$J_{00} = A_0^2 |f_0|^2 \left\{ \beta + \alpha \exp i(2Dk) \left[\frac{1+T^2 \exp i[2(kD+f)]}{1-T^2 \exp i[4(kD+f/2)]} \right] \right\}$$

where

$$2k = \frac{4\pi}{\lambda} \sqrt{\frac{eB+eip}{150.4}}$$

	Fig. IV-5	Fig. IV-6	Fig. IV-7
Face	(100)	(110)	(111)
θ	2.6°	2.6°	5.0°
Surface Debye temperature	110°K	110°K	110°K
f	0.0	0.0	0.0
eip	17	17	17
$\lvert f_{(0)} \rvert^2$	1.0	1.0	1.0
A_0^2	J_0	J_0	J_0
S	.0001	.0001	.0001

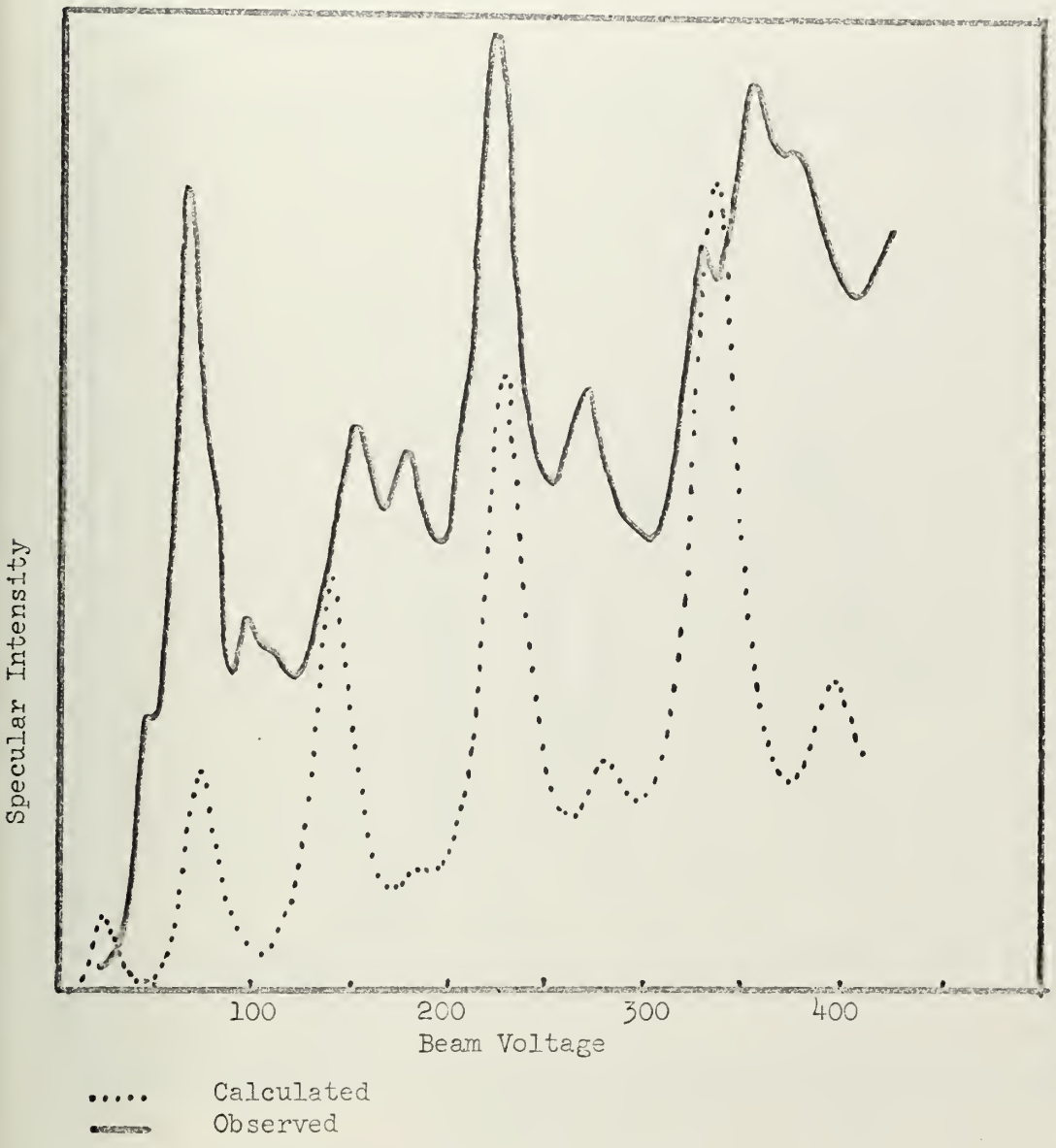

Fig. IV-5. Pt(100) specular intensity recording compared to pseudo-kinematical calculations

Fig. IV-6. Pt(110) specular intensity recording compared to pseudo-kinematical calculations

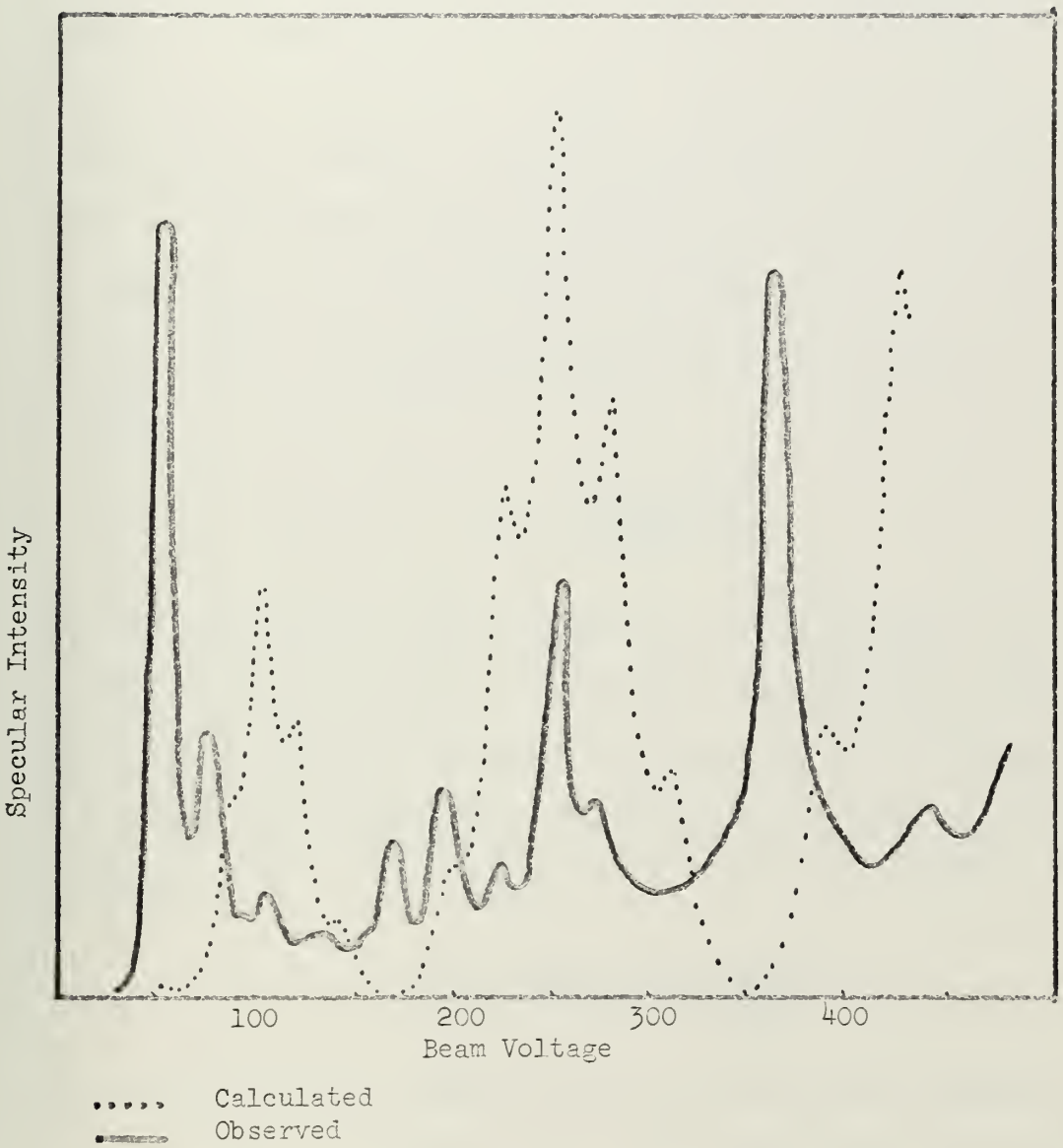

Fig. IV-7. Pt(111) specular intensity recording compared to pseudo-kinematical calculations

V. TEMPERATURE DEPENDENCE OF THE SPECULAR INTENSITY (DEBYE-WALLER EFFECT)

A. Experimental Results

The measurement of the temperature dependence of the specular reflection was carried out by simultaneous recording of the temperature and specular intensity. This was described briefly in Section II.A.7. The background intensity which was also recorded was independent of temperature within our experimental accuracy. The difference between these two recordings, the specular intensity and the background intensity, was taken to be the diffraction spot intensity (I_{diff}, see Section II.A.7). Plots of $\log_{10}(I_{diff})$ vs T°C resulted in straight lines (Fig. V-1). The slopes of these lines, $\Delta \log I/\Delta T$, have been measured and recorded as a parameter τ, where

$$\tau = \left(\frac{\Delta \log I}{\Delta T}\right)^{-1}$$

The values recorded for this parameter are listed in Table V-1. This is a useful parameter which can be related to the Debye temperature. The derivation in Appendix B resulted in an equation (B-13) for the amplitude of the diffraction maxima (α). The intensity is proportional to α^2 which is given by,

$$\alpha^2 = \exp -.7834 \frac{ev \times T}{\left(\theta_D\right)^2}$$

Converting to base ten logarithms and determining the temperature derivative of the log of intensity gives a result which can be used in the calculation of an effective Debye θ.

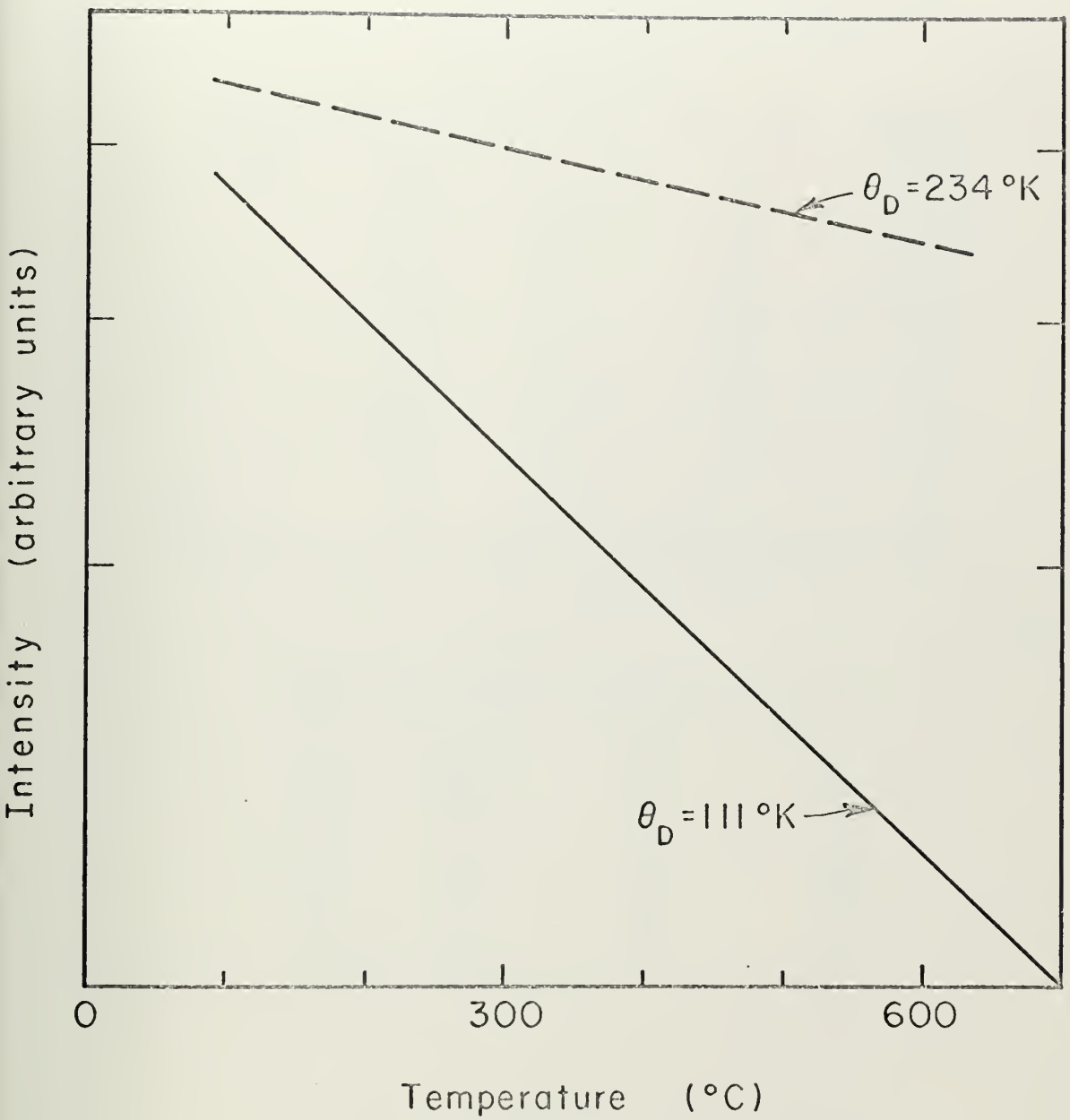

MUB-8769

Fig. V-1. Specular intensity of platinum as a function of temperature

TABLE V-1. DATA

$\cos \theta \cong 1.0$

(111) Face

eB = Beam Voltage

	eB = 35	eB = 63	eB = 175	eB = 195	eB = 250
τ	1036	935	723	778	658
		985	730	650	678
		813	1062	1072	1072
		1355	690	875	1008
		800	810	838	810
		900	870	775	512
		1160	610	733	750
Average	1036	993	785	817	812

(110) Face

eB	τ	eB	τ
25	2260	325	390
172	713	215	795
325	372	18	3500
215	400	66	1380
66	708	215	605
17.5	1565	325	517

(100) Face

eB	τ	eB	τ
21	1930	150	1040
67	1170	217	700
103	987	330	850

$$\frac{d \log_{10} I}{dT} = -.341 \frac{ev}{(\theta_D)^2}$$

The definition of τ allows the experimental data to be converted directly into effective Debye temperature, θ_D,

$$\theta_D = +\sqrt{.341 \times ev \times \tau}$$

The Debye temperatures calculated in this manner are shown in Fig. V-2. The values of the effective Debye temperature are a function of the beam voltage converging to the bulk value at high electron energies.

B. Analysis of Results

A formula for the Debye Waller effect is derived. This result is used in Appendix A to derive an equation which calculates the specular intensity of a diffraction pattern. With reference to Eq. (A-3) we can simplify in such a manner that

$$I = |f_o^2| A_o^2 \{\beta + \alpha M\}^2 \qquad \text{(V-1)}$$

where M is a complex number equal to

$$M = \exp i(2Dk) \left[\frac{1 + T^2 \exp i[2(kD + \phi)]}{1 - T^2 \exp i[4(kD + \frac{\phi}{2})]} \right] \qquad \text{(V-2)}$$

for a major intensity maxima, i.e., those predicted from 3D kinematic theory, $2Dk \simeq N2\pi$ and $|M|$ can be estimated as

$$|M| = \frac{1 + T^2}{1 - T^2} \qquad \text{(V-3)}$$

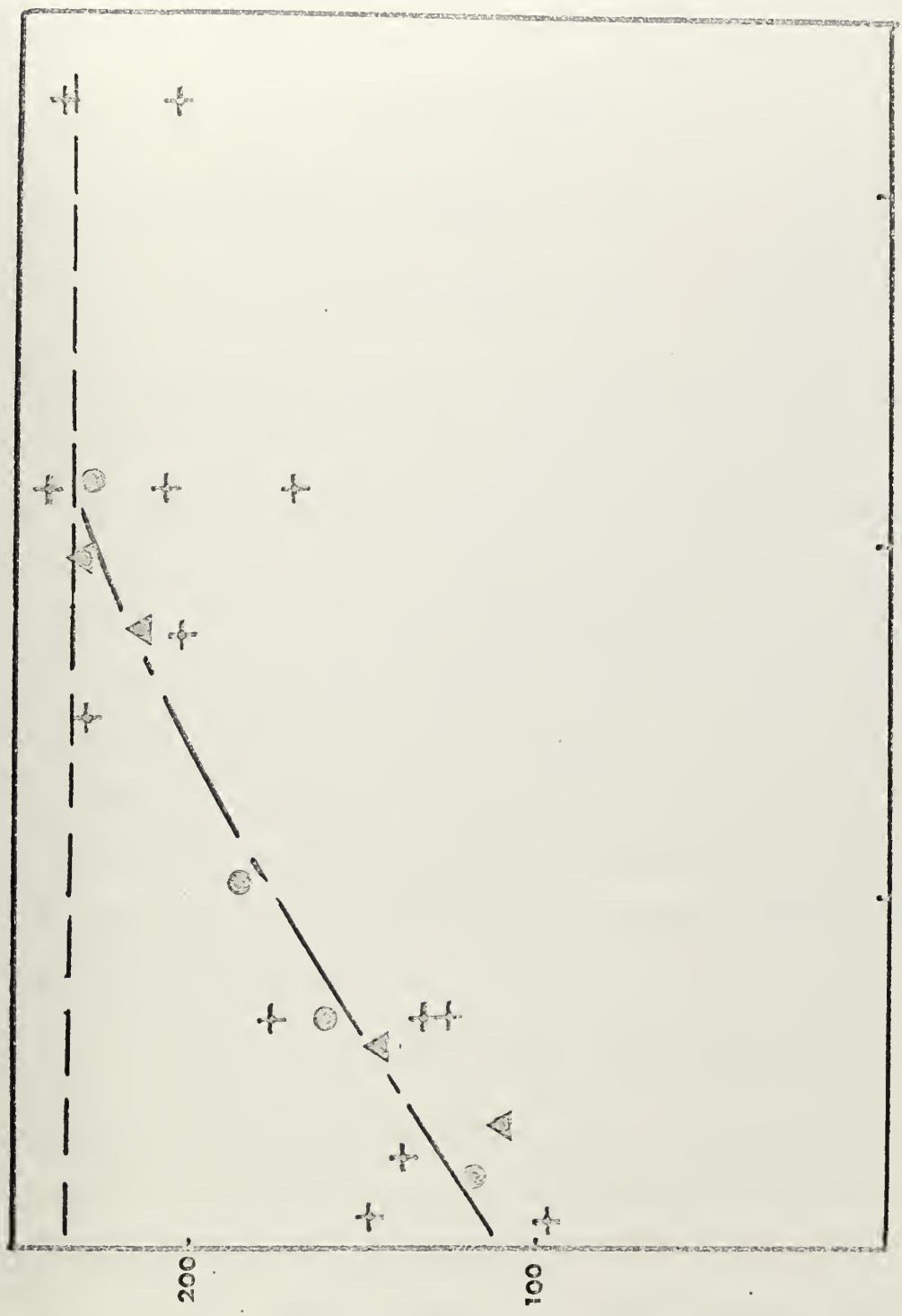

Fig. V-2. Effective Debye temperature as a function of electron beam voltage

For large penetration (high energy) $T \rightarrow 1$ and $|M|$ becomes much larger than unity so that

$$I \simeq |f_0|^2 A_0^2 M^2 \alpha^2 \qquad \text{(V-4)}$$

For zero penetration (low energy) $T \rightarrow 0$ and

$$I = |f_0|^2 |A_0|^2 \{\beta + \alpha\} \qquad \text{(V-5)}$$

We would expect the temperature effect on the intensity (Debye-Waller factor) to be a measure of bulk properties as the energy is increased. At low voltages we should expect an effective Debye temperature composed of a mixture of surface and bulk components. At lowest electron energies θ_D approaches the true surface Debye temperature. A model which takes into account the fractional contributions of the surface and bulk atoms to the experimentally observed θ_D may also be used to determine the surface Debye temperature. The use of such a model can be very important since at low electron energies the θ_D value is very sensitive to the inner potential value used in the calculation. In Eq. (B-13) of the Appendix, the term, eV, is given by

$$eV = \text{beam voltage} + \text{inner potential}$$

Changing the inner potential or neglecting it entirely makes very little difference in the calculated θ_D at high electron energy but at low energy the corrections become appreciable.

The factors listed in Table V-2 are inner potential correction factors. Multiply the Debye temperature, θ_D, calculated without inner potential correction, to correct for the presence of an inner potential

$$\theta_{D_{eff}} = \theta_{D_{(\text{no inner potential})}} \left(\frac{eB + eip}{eB}\right)^{1/2} \qquad \text{(V-6)}$$

eB = beam voltage

eip = inner potential

TABLE V-2

eb \ eip	0	10	20	30
250	1.0	1.02	1.04	1.06
200	1.0	1.02	1.05	1.07
150	1.0	1.03	1.06	1.10
100	1.0	1.05	1.10	1.14
50	1.0	1.09	1.18	1.26

The best fit of the data at high energies appears to be with eip = 0.0. Therefore, the data in Fig. V-2 has been presented without any inner potential corrections.

C. Discussion

It is obvious that the electron energy determines the penetration of the electron into the lattice. At lower energies the beam penetrates less distance into the lattice allowing us to sample the properties of the surface atoms. The effective Debye temperature for low voltages is then more closely related to the surface value.

A difference in the experimental values of the bulk and surface Debye temperatures is expected as a result of theoretical calculations. Clark, Herman and Wallis[28] have shown that the effect of creating a free surface on the atoms in a single crystal is to soften the potential about the surface atoms. This leads to a larger amplitude of oscillation and a lower Debye temperature.

From the measured effective Debye-Waller factors the effective Debye temperatures can be calculated. The effect of the inner potential correction on the experimental data has been discussed. The model which is introduced in Appendix A can also be used to calculate the surface Debye temperature. Both the extrapolation of the experimental determination and the calculations using our model indicate that the surface Debye temperature is 110°K ± 10°K. This leads to an amplitude of oscillation $\langle u^2 \rangle^{1/2}$ which is approximately twice the bulk value.

VI. CONCLUSIONS

A. A low energy electron diffraction study of the low index faces [(100), (110) and (111)] of platinum single crystals has been carried out. The temperature range of investigation was 25°C to 1300°C. These surfaces were investigated in ultra high vacuum and in the presence of different gases. Several ordered surface structures were detected on all three faces of platinum which formed as a function of temperature under the different ambient conditions.

A high temperature anneal of platinum may lead to the irreversible formation of an unreactive disordered surface structure which gives rise to ring-like diffraction patterns.

B. The atoms on the surface of a crystal have a thermal vibration of greater amplitude than the atoms in the bulk. This was determined from the temperature dependence of the specular electron beam intensity (Debye-Waller factor). The amplitude of oscillation $\langle u^2 \rangle^{1/2}$ can be related to the Debye temperature of the surface. The experimental value for the surface Debye temperature is 110°C, or approximately one-half the bulk value. This value appears to be roughly the same for the three faces studied.

C. The specular intensity of a platinum diffraction pattern has been measured as a function of beam voltage. Several properties of these curves which were obtained for the (100), (110), (111) faces could be explained using a pseudo-kinematical description of electron scattering.

ACKNOWLEDGMENTS

My personal gratitude and thanks are reserved for my family, Miriam, Matthew, Andrew and Jonathan. They deserve as much credit as anyone for standing beside me through these years.

I am grateful for the personal relationships established as a result of this work. Especially Dr. Stig Hagstrom and Joseph Lester, who provided me with much needed encouragement and a great deal of good physical chemistry.

My professional gratitude as a Naval Officer is extended to the U.S. Navy under whose "Advanced Science Program" my availability to complete this work was assured. Special credit is given to the Naval Postgraduate School in Monterey which provided me with an excellent year of pre-requisite studies. Without this support the completion of this program would have been impossible.

My academic and scientific gratitude is extended to the Department of Chemistry and the Inorganic Materials Research Division of the Lawrence Radiation Laboratory for the support granted to me under the guidance of Professor Gabor Somorjai.

Last, but not least, my thanks are extended to the secretarial staff of IMRD, especially Pat Cookson, Charlotte Machen and Sharon Sparks for both their friendship, their cheerful typing of this manuscript and 3,713 cups of coffee.

This work was supported in part by the United States Atomic Energy Commission.

Appendix A

THE CALCULATION OF THE BEAM VOLTAGE DEPENDENCE OF SPECULAR INTENSITY

A. Purpose

The derivation contained in Appendices A and B are carried out to analyse the experimental curves obtained from studies of the beam voltage and temperature dependence of the specularly reflected beam intensity. The specular intensity of a beam of electrons reflected from a single crystal has an unexpected dependence upon the beam voltage. Strong maxima and minima occur which are reproducible, are a function of sample temperature and depend upon angle of incidence. This particular derivation of $I_{(\lambda)}$ results in a computer solution in complex space and the final result is achieved by a magnitude determination of a complex sum. In this manner the formulation allows atomic planes which have properties differing from the bulk or each other to be treated individually. Scattering from planes with bulk properties are treated by convergence relationships. The calculations then allow scattering by an infinite crystal. We consider planes of atoms and specify that the results are only valid for the specular intensity at normal incidence.

B. Approximations Used in the Pseudo-Kinematical Theory

1. Intensity Independent Attenuations

The electron beam is attenuated by two mechanisms in general as it travels through the lattice. These attenuation mechanisms are assumed to be independent of the intensity of the electron beam but depend only upon its energy.

2. Collective Phenomena

One of these attenuation mechanisms is the interaction of the electron beam with the lattice. This can most generally be due to electron-electron interactions (band transitions), electron-phonon interactions, and electron-plasmon interactions. These mechanisms can be taken into account by the use of an absorption coefficient, μ, where the amplitude of the incident beam is reduced by a factor $e^{-\mu x}$ after the beam has traveled a certain distance, x, in the lattice. The attenuation due to this mechanism is only a function of the energy of the beam and the distance that the beam has traveled in the lattice.

3. Amplitude Transmission Factor

The second of the attenuation mechanisms is due to the interaction of the electron with a single atom. This is the effect of the atomic scattering factor upon the complex amplitude. It may include elastic as well as inelastic mechanisms.

When conditions for a diffraction maxima in the 2D surface net are satisfied then the factors $f_{(0)}$, $f_{(\pi)}$ can be considered as "planar amplitude absorption factors" and multiple scattering effects in plane can be included in the calculation of these two factors.

4. Multiple Scattering

The effect of multiple scattering other than in-plane multiple scattering events are exluded (see Fig. A-1). The between plane resonances A are excluded by consideration of the other events. B, C, and D as well as all other combinations have been neglected for the sake of computational simplicity. It is the consideration of these very events which makes the dynamical approach necessary.

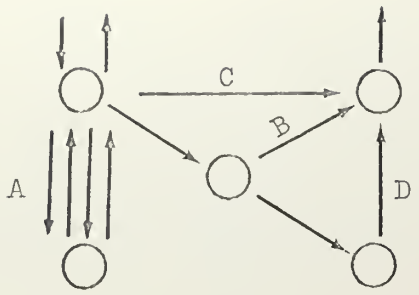

Fig. A-1

C. Derivation

Lander[8] has applied Darwin's[30] solution of scattering by a one dimensional lattice to LEED calculations. The results of this derivation led to the equation for the amplitude scattered into the specular intensity as

$$= A_0 f_0 \left\{ \frac{1}{1-T^2 \exp i(2Dk + 2\phi)} \right\} \qquad \text{(A-1)}$$

where

A_0 is the amplitude of the incident beam

f_0 is the atomic scattering factor for the plane

T can be expressed as the product of two factors. These two factors refer to the attenuation due to adsorption during the transit by the electron of the distance D which is exp-(μD) and the other is the intensity scattered in the forward direction

which may undergo a decrease in amplitude and a phase shift represented by $F_{(\pi)} \exp(i\phi)$

2Dk is the wavelength sensitive term which is equal to $(4\pi/\lambda) \cos\theta$ where θ is the angle of incidence.

The derivation has required T and f_0 to be identical for all atomic planes and has disregarded all Debye-Waller factors. If we assume that for all planes but the first plane we have a Debye-Waller factor, $e^{-M} = \alpha$ then the contribution from these planes would be α times Eq. (A-1). The Debye-Waller factor for the surface plane is different from that for an atom in a bulk plane. The effect of the surface plane is to attenuate the scattering by the bulk planes by $T^2 \exp(2\phi)$ and to add a term $\beta \exp -i(2Dk)$ into the expression for the total scattered amplitude,

$$\psi^0 = A_0 f_0 \left\{ \beta \exp -i(2Dk) + \frac{\alpha T^2 \exp(2\phi)}{1-T^2 \exp i(2Dk+2\phi)} \right\} \qquad \text{(A-2)}$$

Since the scattered intensity is $|\psi^0|^2$, we multiply Eq. (A-2) by the complex conjugate of the phase factor to obtain,

$$\psi^0 = A_0 f_0 \left\{ \beta + \frac{\alpha T^2 \exp i(2Dk + 2\phi)}{1-T^2 \exp i(2Dk + 2\phi)} \right\} \qquad \text{(A-3)}$$

D. Considering a Set of Interpenetrating Lattices

Assume that the electron beam is scattered mainly in the forward direction. Then the penetrating beam is scattered by atoms which are in

equivalent positions in the different atomic planes as shown in Table II-V and Fig. A-2.

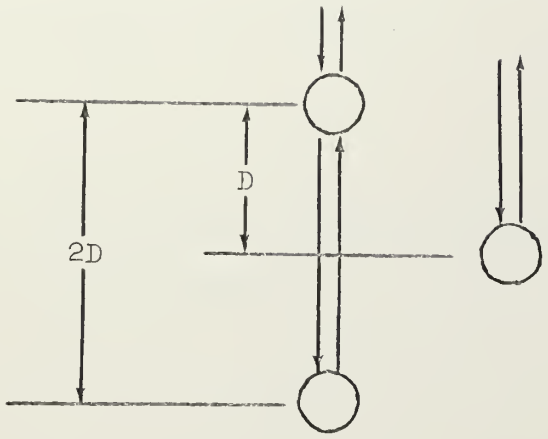

Fig. A-2

For the (100) face of Pt, under these conditions the equivalent atoms are situated in every second atomic plane, 2D apart. As a simplification which limits us to small angles of incidence, we can treat the lattice in this manner. This way for each equivalent set of atoms (1 and 2) we have an independent problem which can be added to calculate the properties of the total beam. Noting that in this particular case, if we let ψ equal the amplitude from one set alone then we can write our equations as

$$\psi_T = \psi_1 + \psi_2$$

At this point we notice that the thermal factor α is the same for the entire second set. ψ_1 is equal to Eq. (A-3). ψ_2 can be written as Eq. (A-1) multiplied by the phase factor exp i(2Dk). We have used the spacing between equivalent planes as 2D. The phase factor arises from the difference

D in spacing between the two equivalent sets of planes. In the final form the equation for the (100) face and (110) face is

$$I_{00} = A_0^2 |f_0|^2 \left\{ \beta + \alpha \exp i(2Dk) \left[\frac{1 + T^2 \exp i\left[2(kD + \phi)\right]}{1 - T^2 \exp i\left[4\left(kD + \frac{\phi}{2}\right)\right]} \right] \right\}^2 \qquad (A\text{-}4)$$

For the (111) face a modification is made for the three equivalent sets of the fcc lattice in the same manner.

Appendix B

The Calculation of the Debye-Waller Effect

1. The Debye-Waller Factor for a Single Plane of Atoms

In this section the Debye-Waller factor will be derived in a form not usually encountered. This specific form is required for use in the intensity calculations derived in Appendix A and the analysis of data in Section V. The results are consistent with other more traditional derivations and are nothing more than a special application. The necessity of this specific method will be apparent later on in the application of the formula to real problems.

The assumptions for this derivation start with a two dimensional lattice plane which is placed perpendicular to the incident electron beam. This is the same as in Appendix A where we only consider two special cases of forward and backward scattering. We treat the atoms in the plane and look at the effect of thermal disorder upon the intensity (Debye-Waller effect).

The position of each atom in this plane can be given by the vector equation from an arbitrary reference.

$$\vec{r}_{ij}(T) = \vec{r}_{ij} + \vec{u}_{ij}(T) \qquad \text{(B-1)}$$

The criteria that these atoms lie in the same plane can be satisfied by the equation,

$$\langle \vec{r}_{ij}(T) \rangle_T \cdot \hat{N} = b \qquad \text{(B-2)}$$

or

$$\vec{r}_{ij} \cdot \hat{N} = b \quad \text{since} \quad \langle \vec{r}_{ij}(T) \rangle_T = \vec{r}_{ij} \qquad \text{(B-3)}$$

where $\hat{N}$ is the unit vector normal to the plane and b is a constant.

The bracket notation will refer to an average value over the independent parameter listed as a subscript to the bracket. It is assumed that the time scale of the electron scattering event is short compared to the period of the lattice vibrations. Figure B-1 shows the time in seconds required for an electron of energy (eV) to travel 10Å calculated from the equation $T = 10\sqrt{\frac{m_e}{2eV}}$.

Therefore, the effect of the thermal vibrations is to introduce randomness in the positions of the atoms. Equation (B-1) then gives the position of the ith, jth atom during the scattering event at time T.

This effect can be visualized by looking at the relationship in the scattering from a displaced atom as compared to its equilibrium position.

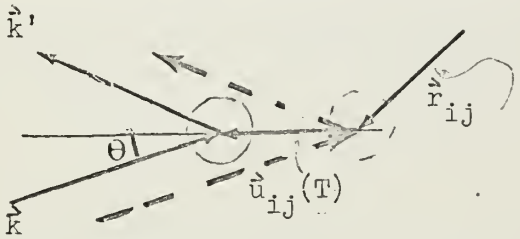

The diffraction equations are calculated for the atom at position $\vec{r}_{ij}$. The effect of the thermal oscillation is to introduce a phase difference ϕ equal to;

$$\phi = \vec{k} \cdot \vec{u}_{ij}(T) - \vec{k}' \cdot \vec{u}_{ij}(T) \qquad \text{(B-4)}$$

or

$$\phi = \Delta\vec{k} \cdot \vec{u}_{ij}(T) \qquad \text{where } \Delta k = 2k \cos\theta$$

For our derivation we are arbitrarily measuring the specular intensity which fixes the form of $\Delta\vec{k}$.

The amplitude then for each atom ij collected at the specular intensity is then

$$\Psi_{(r)}^{k'} = A_0 f_0 \left[\sum_{ij} \exp i(\Delta\vec{k} \cdot \vec{r}_{ij}) \exp i(\Delta\vec{k} \cdot u_{ij}(t) \right] \qquad \text{(B-5)}$$

Since we are only looking at the specular intensity the term

$\exp i(\Delta\vec{R} \cdot \vec{r}_{ij})$ is the same for all atoms ij. This can be factored from the summation and which is now the term α in Appendix A. The problem is to evaluate

$$f_{ij}\alpha = f_{ij} \sum_{ij}^{N} \exp i(\Delta\vec{k} \cdot \vec{u}_{ij}(T)) \tag{B-6}$$

which picks off the component of $\vec{u}_{ij}(T)$ parallel to $\Delta\vec{k}$. $\Delta\vec{k}$ is perpendicular to the surface for the specular reflection so we can write $\Delta\vec{k} \cdot \vec{u}_{ij}(T)$ as $\Delta k\, u^{\perp}_{ij}(T)$. The ergodic hypothesis allows us to rewrite Eq. (B-5) as

$$f_{ij}\alpha = \sum_{ij}^{N} \exp i\, \Delta k u^{\perp}_{ij}(T) = N \exp i\, \Delta k \ \langle u \rangle_T \tag{B-7}$$

This is nothing more than saying the atomic ensemble average under equilibrium conditions is equal to N times the time average of a single atom.

If we let $i\Delta k \langle u^{\perp} \rangle_T = i\langle p \rangle_T$

then a well known relationship [31,32] states that,

$$\exp i \langle p \rangle_T = \exp - \frac{\langle p^2 \rangle_T}{2} \tag{B-8}$$

We have the result that

$$f_o\alpha = Nf_{ij} \exp - \frac{1}{2} \langle \Delta k u^{\perp} \rangle_T^2 \tag{B-9}$$

where $\Delta k = \frac{4\pi}{\lambda} \cos\theta$

and

$$\alpha = \exp - \frac{8\pi^2 \cos^2\theta}{\lambda^2} \langle u^{\perp} \rangle_T^2 \tag{B-10}$$

The term $\langle u \rangle_T^2$ has been evaluated in the high temperature limit of the Debye model[33] of the lattice as

$$\langle u^{\perp} \rangle_T^2 = \left(\frac{3\hbar h}{Mk}\right)^2 \frac{T}{\theta_D^2} \tag{B-11}$$

which leads to the final formula for α, a function of θ_D, λ, θ and T as,

$$\alpha = \exp - \frac{6N\hbar^2}{Mk} \left(\frac{\cos\theta}{\lambda}\right)^2 \frac{T}{(\theta_D)^2} \tag{B-12}$$

and for platinum in more useable terms as,

$$\alpha_i = \exp - .3917 \frac{eV\,T}{(\theta_D^i)^2} \tag{B-13}$$

where we have used the relationship that $\lambda = \sqrt{\frac{150.4}{eV}}$. α_i is often defined in the literature as

$$\alpha_i = e^{-M}$$

where 2M is the so-called Debye-Waller factor.

The derivation of the amplitude Debye-Waller factor was carried out for one plane because of the properties of the lattice. The motivation was provided by theoretical calculations carried out by Clark, Herman, and Wallis.[28] The perpendicular component of oscillation $\langle u^{\perp} \rangle$ has been calculated and the results of CHW are shown in Fig. B-2. These results are from a nearest-neighbor calculation. The squared amplitude of oscillation differs for the surface plane only and that is about twice the bulk value. The surface value appears to be roughly the same regardless of face. For this reason we have considered that the only plane to be different is the surface plane. The factor for the surface plane in Appendix A is called (β) and for all bulk planes (α). The difference lies in the effective Debye temperature, Eq. (B-12).

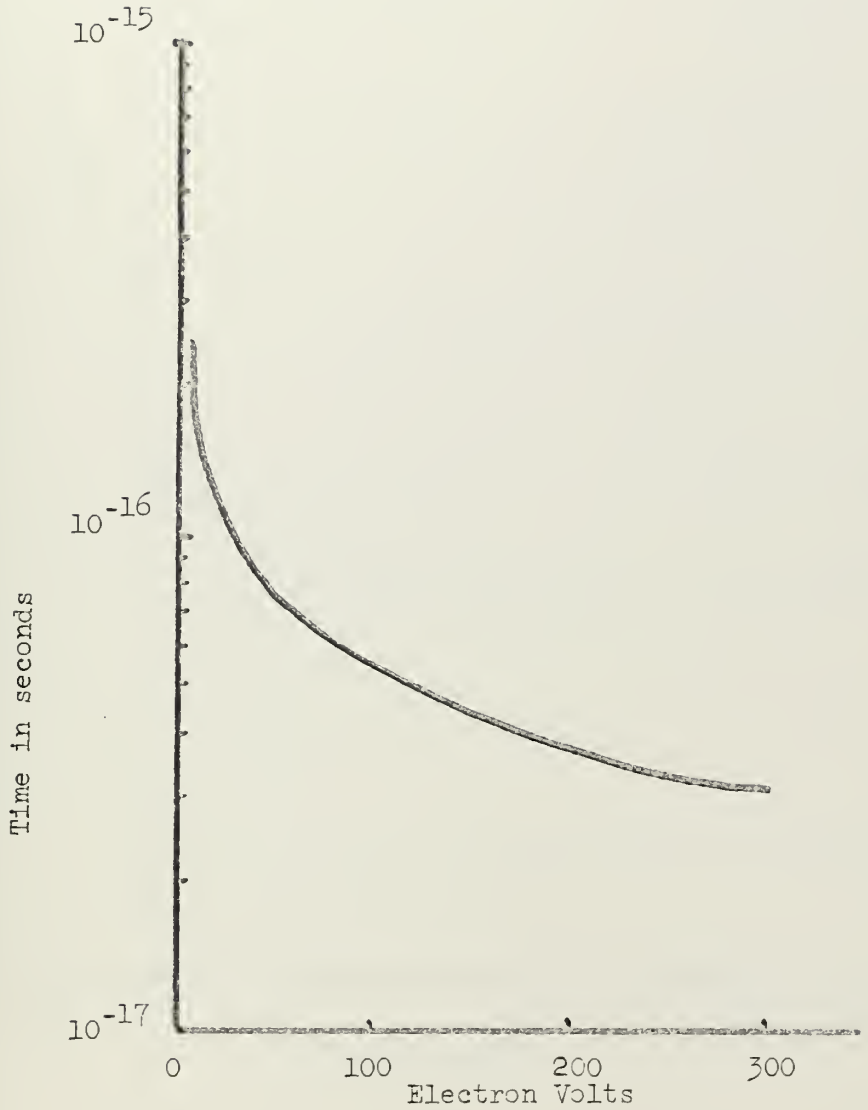

Fig. B-1. Time in seconds for an electron of energy (eV) to travel 10 Angstroms

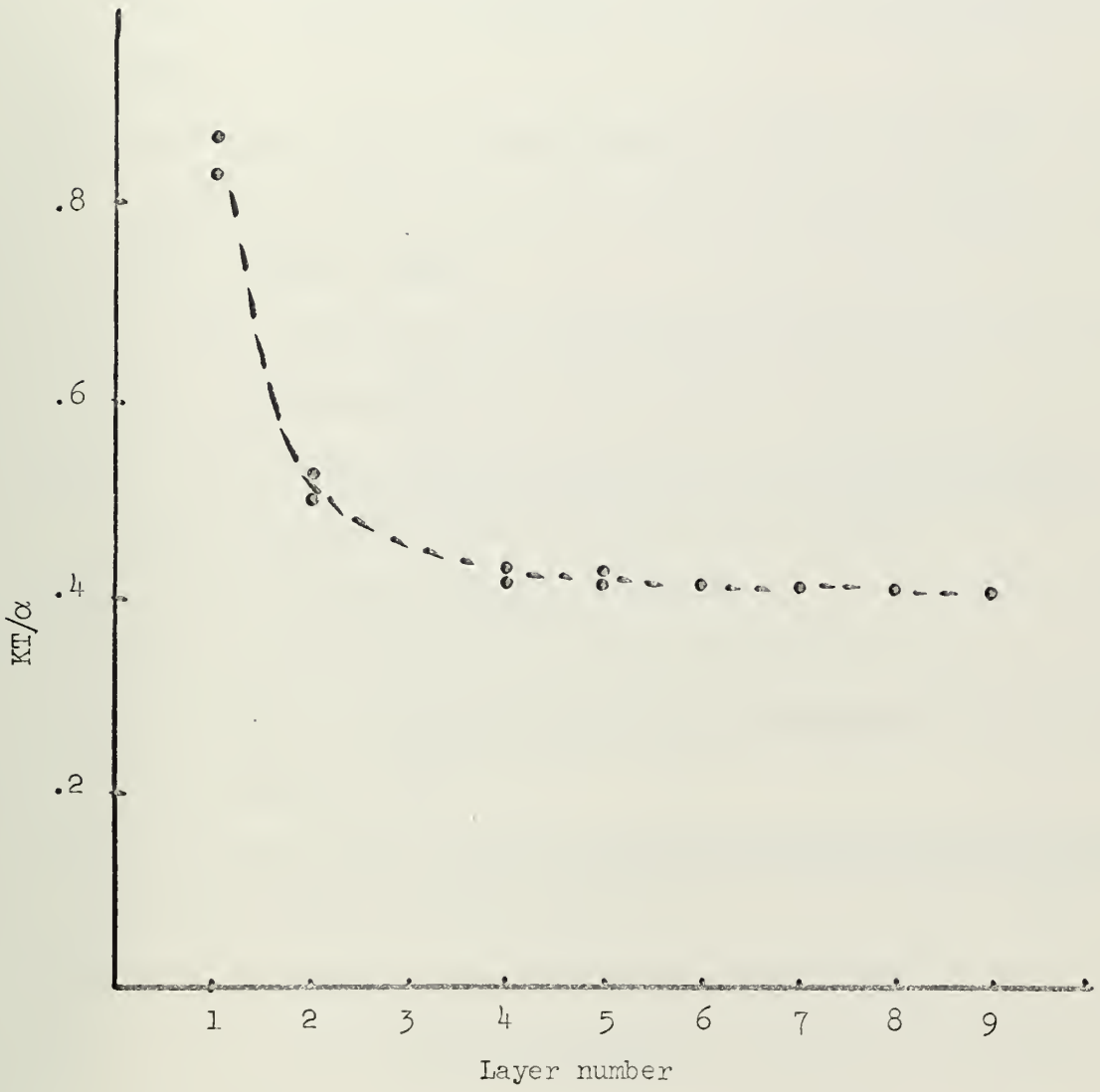

Fig. B-2. Mean-square oscillation $\langle u^2 \rangle$ of atoms in units Kt/α as a function of plane number.[28]

REFERENCES

1. L. Germer, The Structure of Crystal Surfaces, Scientific American, March 1965.

2. H. E. Farnsworth, The Clean Single Crystal Approach to Surface Reactions, in Advances in Catalysis, Vol. 15, Academic Press, New York, 1964.

3. C. W. Tucker, Jr., Low-Energy Electron Diffraction Studies of Gas Adsorption on Platinum (100), (110), and (111) Surfaces, J. Appl. Phys. 35, 1897 (1964).

4. C. Kittel, Introduction to Solid State Physics, John Wiley and Sons, Inc., New York, 1965.

5. F. Roseburg, Handbook of Electron Tube and Vacuum Techniques, Addison-Wesley Publishing Company, Reading, Mass., 1965.

6. W. Ehrenberg, Phil. Mag. 18, 878 (1934).

7. Varian Associates, Inc., Palo Alto, California.

8. J. J. Lander in Advances In Solid State Chemistry, Vol. II, MacMillan Co., New York, 1965.

9. H. Bruining, Physics and Application of Secondary Electron Emission, Pergamon Press, New York, 1954.

10. Varian Associates, Inc., LEED Manual, Vols. I and II.

11. R. W. G. Wycoff, Crystal Structures, Interscience Publishers, New York, 1963.

12. G. N. Lewis, M. Randall, K. S. Pitzer, L. Brewer, Thermodynamics, 2nd. Ed., McGraw-Hill Book Co., New York, 1961.

13. L. Brewer, G. M. Rosenblatt, Dissociation Energies of Gaseous Metal Dioxides, Chem. Revs., 61, 257 (1961).

14. L. Brewer, (Inorganic Materials Research Division, Lawrence Radiation Laboratory, Berkeley, California) private communication, May 1967.

15. J. L. Margrave, Physico-Chemical Measurements at High Temperature, Butterworths, Washington, D.C., 1959.

16. H. B. Lyon, G. A. Somorjai, Low Energy Electron Diffraction of the Clean (100), (111) and (110) Faces of Platinum, J. Chem. Phys., 46, 2539 (1967).

17. E. A. Wood, Vocabulary of Surface Crystallography, J. Appl. Phys., 35, 1306 (1964).

18. A. Guinier, X-Ray Diffraction, W. H. Freeman Co., San Francisco, 1963.

19. D. G. Fedak and N. A. Gjostein, A Low Energy Electron Diffraction Study of the (100), (110) and (111) Surfaces of Gold, Acta. Met., 15, 827 (1967).

20. A. V. MacRae, Adsorption of Oxygen on the {111}, {100}, and {110} Surfaces of Nickel, Surface Sci., 1, 319 (1964).

21. R. L. Park, Sandia Corporation, Alberquerque, New Mexico, work in progress.

22. E. G. McRae, Multiple-Scattering Treatment of Low-Energy Electron Diffraction Intensities, J. Chem. Phys., 45, 3258 (1966).

23. E. Bauer, Crystal Physics Division, Naval Ordnance Laboratory, China Lake, California, to be published.

24. D. S. Boudreaux and V. Heine, Band Structure Treatment of Low Energy Electron Diffraction Intensities, to be published.

25. R. W. James, The Optical Principles of the Diffraction of X-Rays, G. Bell and Sons, Ltd., London, 1965.

26. J. W. May and L. N. Germer, Adsorption of Carbon Monoxide on a Tungsten (110) Surface, J. Chem. Phys., 44, 2895 (1966).

27. H. B. Lyon and G. A. Somorjai, Surface Debye Temperatures of the (100), (111) and (110) Faces of Platinum, J. Chem. Phys., 44, 3707 (1966).

28. B. C. Clark, R. Herman and R. F. Wallis, Theoretical Mean Square Displacements for Surface Atoms in Face-Centered Cubic Lattice with Application to Nickel, Phys. Rev. 139, 860 (1965).

29. P. W. Palmberg and T. N Rhodin, Surface Structures of the Clean Au(100) and Ag(100) Surfaces, Phys. Rev., (in press).

30. C. G. Darwin, The Theory of X-ray Reflection, Phil. Mag., 27, 315 (1914).

31. I. Waller, Zur Frage der Einwirkung der Warmebewegung auf die Interferenz von Rontgenstrahlen, Z. fur Physik, 17, 398 (1923).

32. H. Ott, Der EinfluB der temperatur aufche Rontgenstrewng fester Karper nach der Quanten Mechanik, Ann. Physik, 5, 169 (1935).

33. J. M. Ziman, Principles of the Theory of Solids, Cambridge at the University Press, Cambridge, England, 1964.


525
Amfill
YELLOW